DIFFUSION-WEIGHTED MRI OF FIBROUS TISSUE: CONTRIBUTION OF FAT

BY

RAFAEL A. HERNANDEZ

THESIS

Submitted in partial fulfillment of the requirements
for the degree of Master of Science in Mechanical Engineering
in the Graduate College of the
University of Illinois at Urbana-Champaign, 2010

Urbana, Illinois

Adviser:

Professor John G. Georgiadis

ABSTRACT

The goal of this research project was to develop a model that predicts the effect of fat solution on an MRI signal by a DW-GE pulse sequence. The region of interest is a heterogeneous structure inside a 3mmx3mmx9mm voxel, consisting of loosely arranged micron-sized tubes filled with fat. By assuming that the tubes are parallel inside the domain, the region of interest was simplified into a 2D domain (3mmx3mm). The approach towards achieving the main goal of predicting the signal was to then design different random tube configurations for the region of interest. In total, there were 9 configurations made, where the random positions of the tubes were done by hand: 3 sets of 3 configurations for 30, 35, and 45 tubes. In order to simplify the simulation process, the fat and water domains were done separately, taking advantage of the fact that both are independent of each other and can be concatenated during post-processing. A parametric study was first done with the fat domain, where the circular domain was moved horizontally along the 2D region of interest with a b ($ms/\mu m^2$) range of 0.3 to 0.6 in increments of 0.1. Consequently, the water domain simulations were done for each of the configurations with the same b range values. The results indicate that the experimental values would match a configuration of 30 tubes. Also, there is indication that the fat has an arguably negligible contribution to the signal decay. However, this is probably due to how the water domain area is significantly larger to that of the fat, with a ratio of around 9 to 1 for the configurations used.

ACKNOWLEDGEMENTS

Many thanks to Prof. John Georgiadis for his guidance and support throughout my research in understanding the complexity of diffusion MRI, which became particularly challenging at some points. Also, I would like to thank Jiaxi Lu for helping me in understanding how to actually simulate the MRI pulse sequence. Futhermore, the validation of the model presented in this report could not have been done without the help from the LQVE team, providing assistance in acquiring the necessary experimental data. Last, but certainly not least, I would also like to thank Prof. Brian Thomas for his recommendations and guidance throughout the beginning stages of the numerical simulation process.

TABLE OF CONTENTS

NOMENCLATURE

$\boldsymbol{\mu}$: Magnetic moment vector

h: Planck's Constant

$\boldsymbol{J}$: Spin angular momentum vector

K: Boltzmann's Constant

$\boldsymbol{M}$: Magnetization vector

N_s: Number of spins in a proton system

T_1: Longitudinal relaxation time constant

T_2: Transverse relaxation time constant

γ: Gyromagnetic ratio

ABBREVIATIONS AND TERMINOLOGY

ADC: Apparent Diffusion Coefficient

DTI: Diffusion Tensor Imaging

DW-GE: Diffusion Weighted Gradient Echo

IMCL: Intramyocellular Lipid

MRI: Magnetic Resonance Imaging

NMR: Nuclear Magnetic Resonance

PTFE: polytetrafluoroethylene

Tomography: imaging by sections or sectioning, through the use of wave of energy

Voxel: Volume element in MRI (3D pixel)

1. OBJECTIVE

The goal of this research project is to develop a model that predicts the effect of fat solution on an MRI signal by a DW-GE pulse sequence across a heterogeneous structure consisting of loosely arranged micron-sized tubes. The fat is located inside the tubes, and water fills the gaps between the tubes. The figure below shows a conceptualized region of interest, with 35 tubes located randomly within the domain.

Due to limitations in not knowing the actual location and spacing between the tubes in the experimental setup, this project will explore how the signal produced by changing these two parameters compares with respect to the signal produced in the experiment. It is important to note that the model outlined in this report is only one way to approach the problem of accurately simulating the MRI signal. Choosing any amount of tubes within the domain is simply an educated guess, as there might be more or less tubes actually included in the experimental domain.

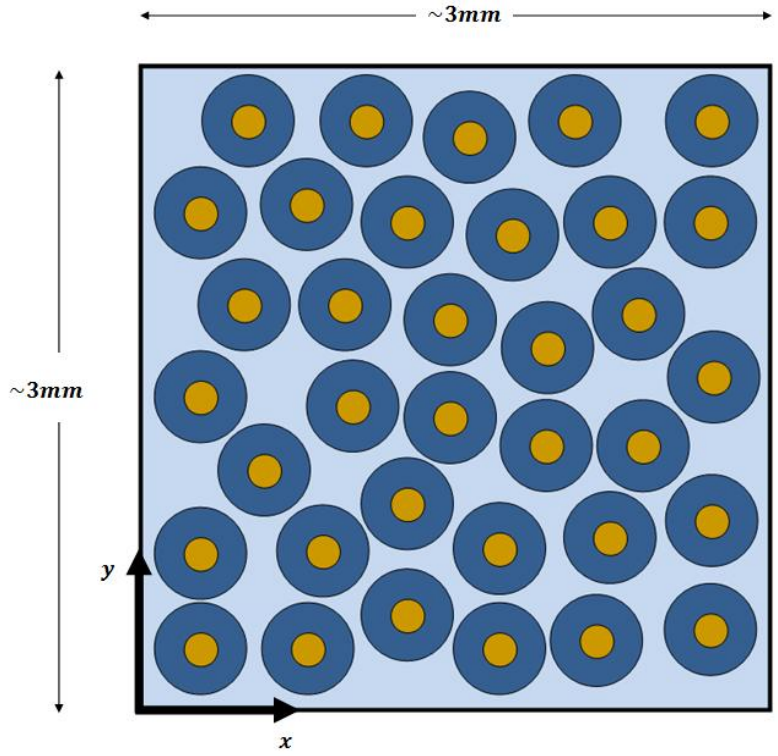

Figure 1.1: Conceptual Domain with 35 Tubes

2. BACKGROUND

The motivation behind this research lies in the study of human skeletal muscle at the fiber level, particularly how the molecular diffusion of water in the tissue is affected with the presence of fat when the muscle is at rest [1], which is then believed to affect muscle quality [2]. To analyze the motion of water in-vivo at the micrometer scale requires a powerful measurement device that is non-invasive, does not affect the natural movement of the water, and is sensitive enough to accurately capture the molecular diffusion occurring in such a small domain. Such a device is the MRI machine.

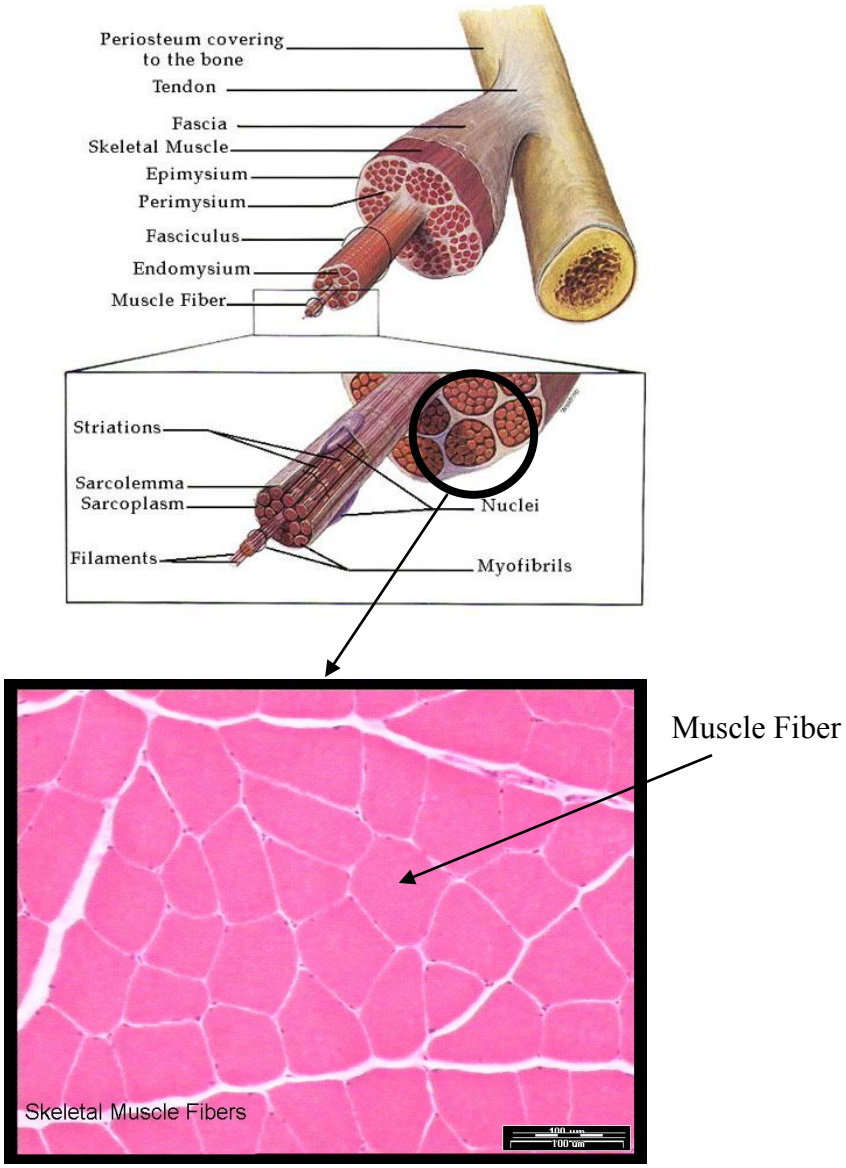

Figure 2.1: Muscle Fiber Location

This report will not go into much detail as to the workings and vast capabilities of an MRI machine, but for the interested reader, the textbook "Principles of Magnetic Resonance Imaging" [4] by Liang and Lauterburg (both current faculty of UIUC) provides a thorough look into the field of magnetic resonance imaging. Most of the technical information in this section originates from that book.

Essentially, the MRI machine measures nuclear magnetic resonance (NMR) signals emitted by an object in the presence of a magnetic field. It is a powerful tomographic imaging device, capable of producing 3D images with a pre-definable resolution. However, here lies a problem when it comes to imaging people in vivo, in that the resolution is directly proportional to the acquisition time, meaning that for a decrease in voxel size, more time is required. As opposed to many, if not all, studies of engineering materials, the analysis of human beings requires protocols to follow and consideration of the comfort of those individuals undergoing measurements inside the machine. The average voxel size used by the LQVE group in muscle acquisition is 3mmx3mmx9mm. This means that it is not possible to distinguish individual muscle fibers, which are around ~50μm in diameter, as well as fat content inside the fibers from the image.

The capabilities of the MRI machine are not restricted to just a visual representation of an object. In fact, it is capable of acquiring NMR signal information that can be used to determine the apparent molecular diffusion of a substance inside a voxel. This is done by using a pulse sequence that changes the spin orientations of the molecule protons in a timely fashion using alterations of the magnetic field, with the intent of then relating the signal change produced by the magnetization diffusion to the movement of the molecules inside the voxel. This is the focus area of Diffusion Tensor Imaging (DTI), where an apparent diffusion tensor is obtained by taking measurements along many directions across the object [3]. The pulse sequence of interest in this project is the Diffusion Weighted Gradient Echo, which will be described in the Phenomena section of the report.

One of the main goals of the Laboratory of Quantitative Visualization in Energetics (LQVE) at UIUC is to make use of the diffusion capturing capabilities of the MRI machine in order to determine skeletal muscle fitness based on NMR signals of muscles at rest (subjects lie down inside the machine without moving). One of the focal points of the research group is the Intra-myocellular lipid (fat) concentration inside the muscle fibers, and how it affects the molecular diffusion acquired using the MRI machine. This leads to the motivation behind the current project, which is to create a model that can predict molecular water diffusivity based on IMCL concentration.

As far as the research team is concerned, this is the first model that intends to do such a thing. The model proposed in this project will be validated with a controlled experiment, where 100μm inner diameter PTFE plastic tubes are filled with an aqueous fat solution made to closely resemble IMCL. These tubes represent the muscle fibers, even though they are twice as large as the diameter of an actual muscle fiber (~50μm), and the fat solution with known concentration represents the IMCL. This is the closest experiment that will be done so far by the research group that resembles muscle fibers and the IMCL, both in size scale and structure.

This project is addressed to researchers in the area of molecular water diffusion of skeletal muscle and its relation to fitness, as well as to those who are in the field of obesity, who can make use of the model to obtain a better understanding of the negative effects of fat in the muscles of people who live a sedentary lifestyle.

3. PHENOMENA

As mentioned in the previous section, the project aims to simulate the Diffusion Weighted Gradient Echo pulse sequence using a model. But, before going further into what this pulse sequence is, it will be beneficial to understand the basic physics of water NMR.

The water molecule consists of an oxygen atom and two hydrogen protons that have nonzero spins. When any charged object spins, it creates a magnetic field around it, and such is the case with hydrogen in water. It is important to note that the spinning of the hydrogen nucleus is independent of the movement of the water molecule, which is the basis for being able to calculate the diffusion using the MRI machine. The spin angular momentum (***J***) and the magnetic moment vector (***μ***) are related to each other by the equation:

$$\vec{\mu} = \gamma \vec{J}$$

where "γ" is the physical constant known as the gyromagnetic ratio, for hydrogen it is equal to 2.675×10^8 rad/s/T .

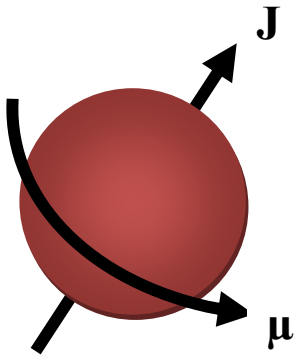

Figure 3.1: Muscle Fiber Location

The concept of bulk magnetization is introduced, which describes the collective behavior of a spin system using a macroscopic magnetization vector ***M***. The vector sum of all the microscopic magnetic moments in a system is equal to ***M*** through the following equation:

$$\vec{M} = \sum_{n=1}^{N_s} \vec{\mu}_n$$

where $\boldsymbol{\mu_n}$ represents the magnetic moment of the *n*th nuclear spin and *Ns* is the total number of spins in the object being imaged [4]. When there is no magnetic field applied and the system is in thermal equilibrium, this summation yields zero. However, when there is a magnetic field B_0 applied to a hydrogen system, the magnitude of the bulk magnetization vector, which lies in the same direction as the magnetic field vector, is described by:

$$M_z^0 = \left|\vec{M}\right| = \frac{\gamma^2 h B_0 N_s}{16\pi^2 K T_s}$$

where h is Planck's constant, K is Boltzmann's constant, and T_s is the absolute temperature of the spin system [4]. The reason for the "z" subscript is purely conventional, since the coordinate system is usually set as having the magnetic field pointing in the "z" direction.

At this point, it is only necessary to understand that when a constant magnetic field is applied to a system of hydrogen protons, the magnetic moment vectors of each proton will be aligned towards the direction of the field. In reality, an almost equal portion of protons will point in the direction opposite the field, but for now we assume all of them are pointing in the same direction, and this will be taken into account in the expressions provided later on in the report.

Once the protons are aligned toward the constant magnetic field, and if an excitation pulse is applied, the system then undergoes a period of free precession and relaxation toward the initial orientation of the magnetic moment. There are two time constants related to this phenomenon: T_1 and T_2. The amount of time it takes for the longitudinal component of the magnetic moment (the "z" direction by convention) to regain 63% of its thermal equilibrium value during free relaxation is defined by T_1. The time it takes for the transverse magnetization to lose 37% of its excited-state magnetization during free relaxation is T_2. A more physical interpretation of these

constants is that T_1 is caused by the magnetic field, forcing the protons to gradually align back, while T_2 is caused by the spin-spin interactions in the transverse direction between the protons. These two time constants appear in the governing equations mentioned later on in the report.

Now there is believed to be enough information to describe what the Diffusion Weighted Gradient Echo pulse sequence is about. The concept behind this is to obtain a signal measurement (voltage inductance) that is capable of capturing the molecular diffusion of water, by means of carefully timed pulses and the intermittent application of magnetic field gradients during a certain amount of time. A simplified pulse sequence is illustrated below,

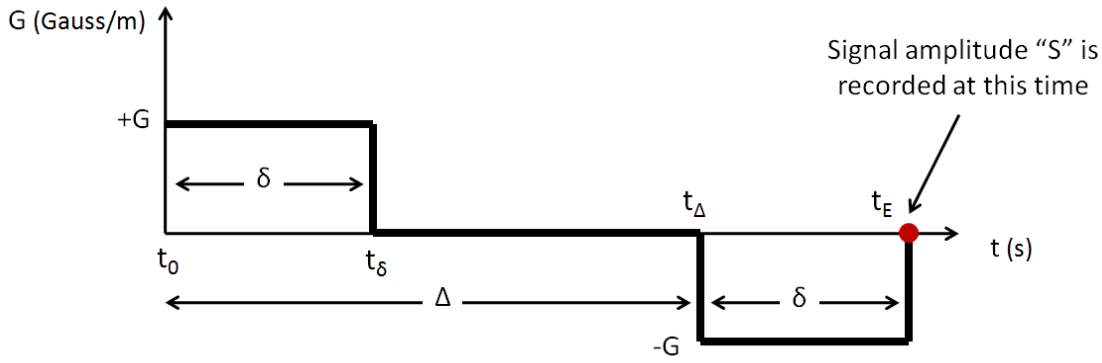

Figure 3.2: Timeline for Simplified DW-GE Pulse Sequence

where,

t_0 = radio frequency pulse ends

t_δ = end of +G pulse

t_Δ = start of -G pulse

t_E = signal acquired ≈ 56ms

γ = gyromagnetic constant for hydrogen

S_0 = signal when "b = 0"

The idea behind the pulse sequence is to de-phase and then re-phase the magnetic moment vectors, while allowing the protons to diffuse freely the entire time. The movement of the molecules will then affect the signal captured at time t_E. This project aims to simulate the sequence for different b values in order to obtain an apparent diffusion coefficient (ADC) as described in the equation [6]:

$$\frac{S(t_E)}{S_0} = e^{-b(ADC)}$$

The parameter b is called the "b factor," and it characterizes the gradient pulses (timing, amplitude, shape) used in the MRI sequence. For this project, the importance of b is that it has a directly proportional relationship with the magnitude of the gradient [5], as shown here:

$$b = \gamma^2 \left(G_{mag}\right)^2 \delta^2 (\Delta - \frac{\delta}{3})$$

The MRI experiment takes measurements based on an array of b values, which will also be employed in the simulations for this project. The idea is to recreate the experiment through simulation and calculate the apparent diffusion coefficient for different arrangements of 30, 35, and 40 tubes.

4. APPROACH/METHODOLOGY

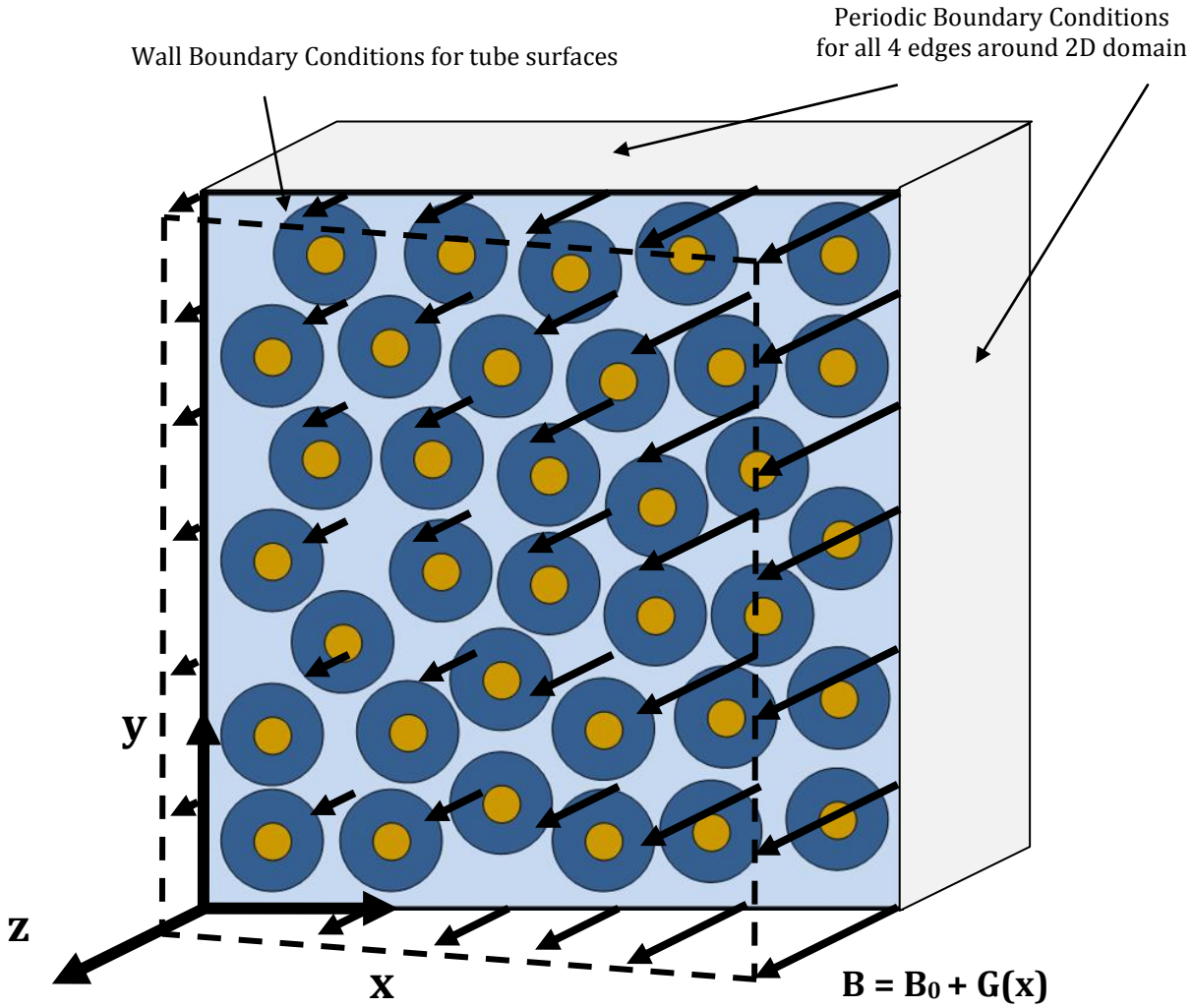

Figure 4.1: Physics and Boundary Conditions for Voxel Domain

The governing equation without Diffusion is as follows:

$$\frac{d\vec{\boldsymbol{M}}}{dt} = \gamma(\vec{\boldsymbol{M}} \times \vec{\boldsymbol{B}})$$

Adding relaxation effects:

$$\frac{dM_Z}{dt} = -\frac{M_Z - M_0}{T_1}$$

$$\frac{dM_{x,y}}{dt} = -\frac{M_{x,y}}{T_2}$$

Becomes the Bloch-Torrey equation including diffusion [7]:

$$\frac{d\vec{\boldsymbol{M}}}{dt} = \gamma\left(\vec{\boldsymbol{M}} \times \vec{\boldsymbol{B}}\right) - \frac{M_x\hat{\boldsymbol{\imath}} + M_y\hat{\boldsymbol{\jmath}}}{T_2} - \frac{M_z - M_z^0}{T_1}\hat{\boldsymbol{k}} + \boldsymbol{\nabla}\cdot\left(\underline{\underline{\mathbf{D}}}\,\boldsymbol{\nabla}\,\vec{\boldsymbol{M}}\right)$$

$$\frac{d\vec{\boldsymbol{M}}}{dt} = \gamma\left(\vec{\boldsymbol{M}} \times \vec{\boldsymbol{B}}\right) - \frac{M_x\hat{\boldsymbol{\imath}} + M_y\hat{\boldsymbol{\jmath}}}{T_2} - \frac{M_z - M_z^0}{T_1}\hat{\boldsymbol{k}} + \mathrm{D}\,\boldsymbol{\nabla^2}\vec{\boldsymbol{M}}$$

If we assume that the thickness of the domain is infinite ($\Delta z \approx \infty$), then the equation above can be simplified to a 2D domain on x and y, yielding:

$$\frac{d\vec{\boldsymbol{M}}}{dt} = \gamma\left(\vec{\boldsymbol{M}} \times \vec{\boldsymbol{B}}\right) - \frac{M_x\hat{\boldsymbol{\imath}} + M_y\hat{\boldsymbol{\jmath}}}{T_2} + \mathrm{D}\left(\frac{\partial^2\vec{\boldsymbol{M}}}{\partial \mathrm{x}^2} + \frac{\partial^2\vec{\boldsymbol{M}}}{\partial \mathrm{y}^2}\right)$$

Since the vector B is parallel to the k direction, the cross product will not have a component in this direction.

$$\vec{\boldsymbol{M}} \times \vec{\boldsymbol{B}} = \begin{bmatrix} \hat{\boldsymbol{\imath}} & \hat{\boldsymbol{\jmath}} & \hat{\boldsymbol{k}} \\ M_x & M_y & M_z \\ 0 & 0 & B_z \end{bmatrix} = M_y B_z\hat{\boldsymbol{\imath}} - M_x B_z\hat{\boldsymbol{\jmath}}$$

$$\frac{\partial M_x}{\partial t} = \gamma B_z M_y - \frac{M_x}{T_2} + D\left(\frac{\partial^2 \mathrm{M_x}}{\partial \mathrm{x}^2} + \frac{\partial^2 \mathrm{M_x}}{\partial \mathrm{y}^2}\right)$$

$$\frac{\partial M_y}{\partial t} = -\gamma B_z M_x - \frac{M_y}{T_2} + D\left(\frac{\partial^2 \mathrm{M_y}}{\partial \mathrm{x}^2} + \frac{\partial^2 \mathrm{M_y}}{\partial \mathrm{y}^2}\right)$$

where for the rotational frame of reference,

$$B_z = g \cdot x$$

The above system of parabolic partial differential equations can be rearranged in a more general form:

$$d_{11}\frac{\partial M_x}{\partial t} + d_{12}\frac{\partial M_y}{\partial t} - c_{11}\nabla^2 M_x - c_{12}\nabla^2 M_y + a_{11}M_x + a_{12}M_y = f_1$$

$$d_{21}\frac{\partial M_x}{\partial t} + d_{22}\frac{\partial M_y}{\partial t} - c_{21}\nabla^2 M_x - c_{22}\nabla^2 M_y + a_{21}M_x + a_{22}M_y = f_2$$

$$\begin{pmatrix} d_{11} & d_{12} \\ d_{21} & d_{22} \end{pmatrix} = \begin{pmatrix} 1 & 0 \\ 0 & 1 \end{pmatrix}, \qquad \begin{pmatrix} c_{11} & c_{12} \\ c_{21} & c_{22} \end{pmatrix} = \begin{pmatrix} D & 0 \\ 0 & D \end{pmatrix},$$

$$\begin{pmatrix} a_{11} & a_{12} \\ a_{21} & a_{22} \end{pmatrix} = \begin{pmatrix} \frac{1}{T_2} & -\gamma B_z \\ \gamma B_z & \frac{1}{T_2} \end{pmatrix}, \qquad \begin{pmatrix} f_1 \\ f_2 \end{pmatrix} = \begin{pmatrix} 0 \\ 0 \end{pmatrix}$$

$$\alpha = \frac{1}{T_2}, \qquad \beta = \gamma B_z, \qquad \begin{pmatrix} a_{11} & a_{12} \\ a_{21} & a_{22} \end{pmatrix} = \begin{pmatrix} \alpha & -\beta \\ \beta & \alpha \end{pmatrix}$$

The following figure illustrates the timeline for the simplified pulse sequence:

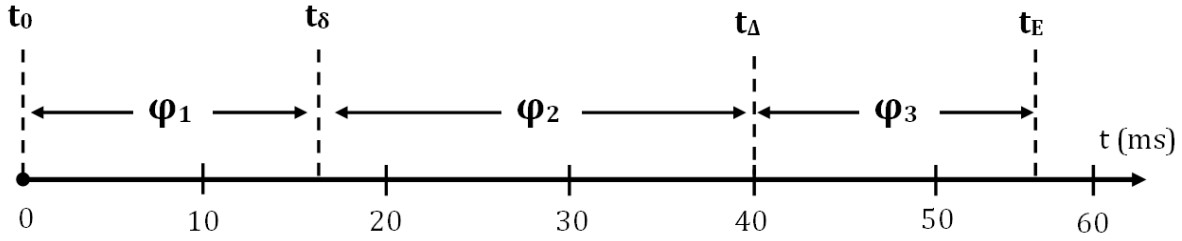

Figure 4.2: Timeline for DW-GE Simplified Pulse Sequence

$$\boldsymbol{\varphi_1}\ (0 \le t < t_\delta), \qquad \alpha = 1/T_2\,, \qquad \beta = \gamma(g.x)$$

$$\boldsymbol{\varphi_2}\ (\mathrm{t}_\delta \le \mathrm{t} < \mathrm{t}_\Delta), \qquad \alpha = 1/T_2\,, \qquad \beta = 0$$

$$\boldsymbol{\varphi_3}\ (t_\Delta \le t \le t_E), \qquad \alpha = 1/T_2\,, \qquad \beta = \gamma(-g.x)$$

$$\frac{\partial M_x}{\partial t} - D\nabla^2 M_x + \alpha M_x - \beta M_y = 0$$

$$\frac{\partial M_y}{\partial t} - D\nabla^2 M_y + \alpha M_y + \beta M_x = 0$$

The signal at any time is calculated as:

$$\frac{S(t)}{S(0)} = \frac{\sqrt{[M_{x\,tot}(t)]^2 + [M_{y\,tot}(t)]^2}}{\text{Area}}$$

Table 4.1: Constants Involved for Simulation

Constant	Value
Gyromagnetic ratio for hydrogen (rad/ms*mT)	267.5
δ (ms)	16
Δ(ms)	40
Time for echo (ms)	56

Table 4.2: Medium Properties

Properties	Medium I	Medium II	Medium III
Material	Pure Water	Lipid (Fat)	Ultramicrobore PTFE
Self-Diffusivity (μm²/ms)	2.2	1.64	-
T_2 (ms)	2000	127	-

5. PROGRAM VALIDATION

The software package used is COMSOL Multiphysics 3.5. This software allows the user to have direct access to the governing partial differential equations it uses for the FEM analysis. Considering that the equations for this project are not in classical form, it is important to use a software package that allows the user to modify the equations being solved to suit this project.

In order to verify that the program has the potential to work for the intended simulations, a 2D ODE test problem is run on COMSOL. It consists of solving for the evolution of the components of the magnetization vector as a function of time during the pulse sequence, without including diffusion. The following circular domain is used, which corresponds to the inside of a tube, located at 50micrometers from the origin in both the x+ and y+ directions:

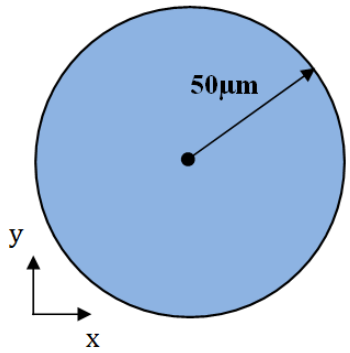

Figure 5.1: Circle Fat Domain for Simulation

Recall that the governing equations for each time region, neglecting diffusion, are as follows:

Phi 1:

$$\frac{dM_x}{dt} = -\left(\frac{1}{T_2}\right)M_x + (\gamma g x)M_y \qquad \frac{dM_y}{dt} = -(\gamma g x)M_x - \left(\frac{1}{T_2}\right)M_y$$

Phi 2:

$$\frac{dM_x}{dt} = -\left(\frac{1}{T_2}\right)M_x \qquad \frac{dM_y}{dt} = \left(\frac{1}{T_2}\right)M_y$$

Phi 3:

$$\frac{dM_x}{dt} = -\left(\frac{1}{T_2}\right)M_x - (\gamma g x)M_y \qquad \frac{dM_y}{dt} = (\gamma g x)M_x - \left(\frac{1}{T_2}\right)M_y$$

An analytical solution to these equations can be determined, giving rise to the equations below (details in derivation shown in Appendix A). The initial condition (at t=0) is set to "1" for Mx and "0" for My. The reason for this initial condition is that we are only interested in the dimensionless signal value, given by S/S_0. At the beginning of the pulse sequence, the magnetization vectors point only along the x axis (hence My being equal to zero). The function h(x) is the vertical length of the domain at position x, introduced in order to calculate the total Mx and My for the circle domain. As mentioned before, the derivations for the equations can be found in Appendix A.

$$h(x) = 2\sqrt{2500 - (x-50)^2}\ for\ circle$$

Phi 1: $0 < t \leq t_\delta$

$$M_{x\,tot}(t) = e^{-\left(\frac{t}{T_2}\right)} \int_{x_0}^{x} h(x)\cos(\gamma g x t)\,dx$$

$$M_{y\,tot}(t) = -e^{-\left(\frac{t}{T_2}\right)} \int_{x_0}^{x} h(x)\sin(\gamma g x t)\,dx$$

Phi 2: $t_\delta < t \leq t_\Delta$

$$M_{x\,tot}(t) = e^{-\left(\frac{t}{T_2}\right)} \int_{x_0}^{x} h(x)\cos(\gamma g x t_\delta)\,dx$$

$$M_{y\,tot}(t) = -e^{-\left(\frac{t}{T_2}\right)} \int_{x_0}^{x} h(x)\sin(\gamma g x t_\delta)\,dx$$

Phi 3: $t_\Delta < t \leq t_E$

$$M_{x\,tot}(t) = e^{-\left(\frac{t+t_\delta}{T_2}\right)} \int_{x_0}^{x} h(x)\{\cos(\gamma g x t_\delta)\cos[-\gamma g x(t-t_\Delta)] + \sin(\gamma g x t_\delta)\sin[-\gamma g x(t-t_\Delta)]\}dx$$

$$M_{y\,tot}(t) = e^{-\left(\frac{t+t_\delta}{T_2}\right)} \int_{x_0}^{x} h(x)\,[-\cos(\gamma g x t_\delta)\sin[-\gamma g x(t-t_\Delta)] + \sin(\gamma g x t_\delta)\cos[-\gamma g x(t-t_\Delta)]]dx$$

For all time regions, the signal is expressed as the following:

$$\frac{S(t)}{S(0)} = \frac{\sqrt{[M_{x\,tot}(t)]^2 + \left[M_{y\,tot}(t)\right]^2}}{\text{Area}}$$

The following table shows the numerical values used for the simulations:

Table 5.1: Numerical Parameters and Constants

Parameters/Constants	Value
Gyromagnetic ratio for hydrogen (rad/ms*mT)	267.5
g, gradient magnetic field (mT/μm)	2.6×10^{-5}
t_δ (ms)	16
t_Δ(ms)	40
t_E (ms)	56
T2 for lipid (ms)	127
Mx initial (mT)	1
My initial (mT)	0
Wall boundary condition, Dirichlett	**M**=0
Time step (ms)	0.001

The following is the mesh generated in COMSOL. The domain is divided into four subdomains in order to have a smoother mesh. The square side lengths are equal to the radius of the circle (50μm).

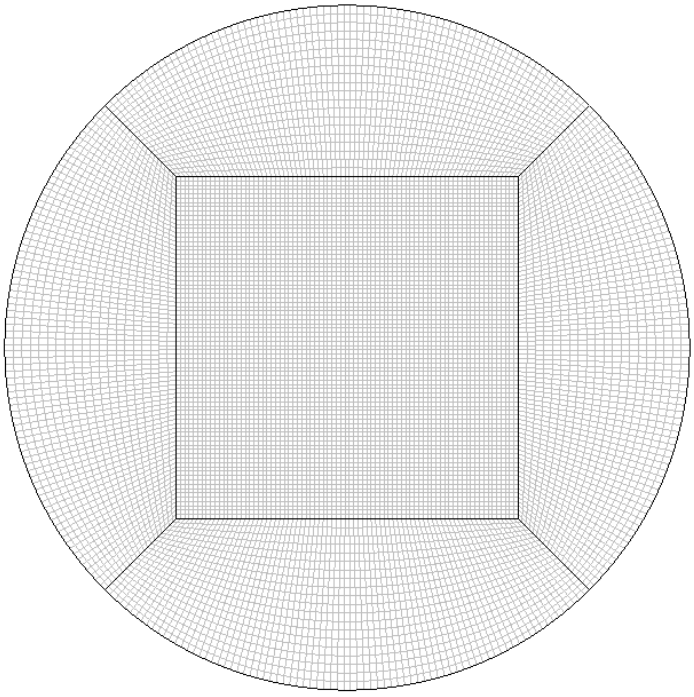

Figure 5.2: Circle Domain Mesh

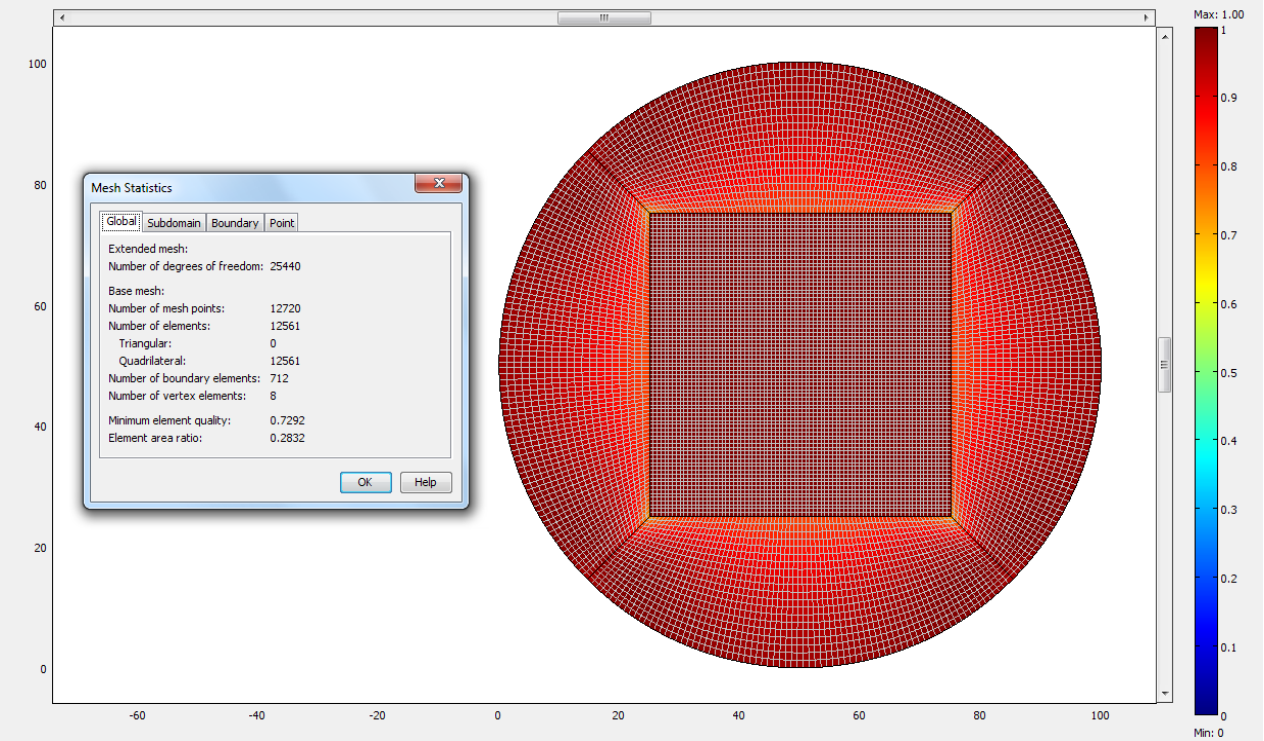

Figure 5.3: Circle Domain Mesh Quality and Statistics

The following graph shows the results of the simulation without including diffusion effects:

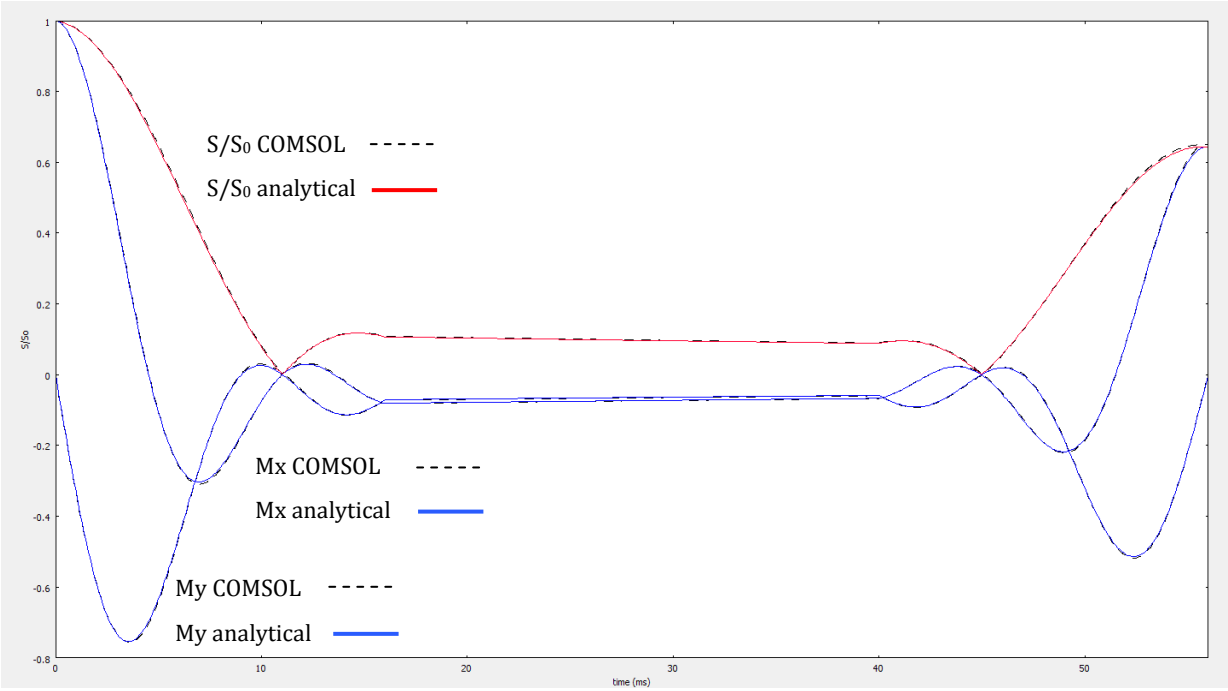

Figure 5.4: Simulation without Diffusion

Now we repeat the above simulation but including diffusion of 2.2 μm²/ms, introduced in the governing equations shown below.

Phi 1:

$$\frac{dM_x}{dt} = -\left(\frac{1}{T_2}\right)M_x + (\gamma g x)M_y + D\nabla^2 M_x \qquad \frac{dM_y}{dt} = -(\gamma g x)M_x - \left(\frac{1}{T_2}\right)M_y + D\nabla^2 M_y$$

Phi 2:

$$\frac{dM_x}{dt} = -\left(\frac{1}{T_2}\right)M_x + D\nabla^2 M_x \qquad \frac{dM_y}{dt} = -\left(\frac{1}{T_2}\right)M_y + D\nabla^2 M_x$$

Phi 3:

$$\frac{dM_x}{dt} = -\left(\frac{1}{T_2}\right)M_x - (\gamma g x)M_y + D\nabla^2 M_x \qquad \frac{dM_y}{dt} = (\gamma g x)M_x - \left(\frac{1}{T_2}\right)M_y + D\nabla^2 M_x$$

After running the simulation in COMSOL, the following graph is obtained, showing a decay in the signal which was to be expected. The solid lines are for the non-diffusion case. The diffusion seems to have a significant effect during the rephasing time region (right-most region), as opposed to the previous time regions.

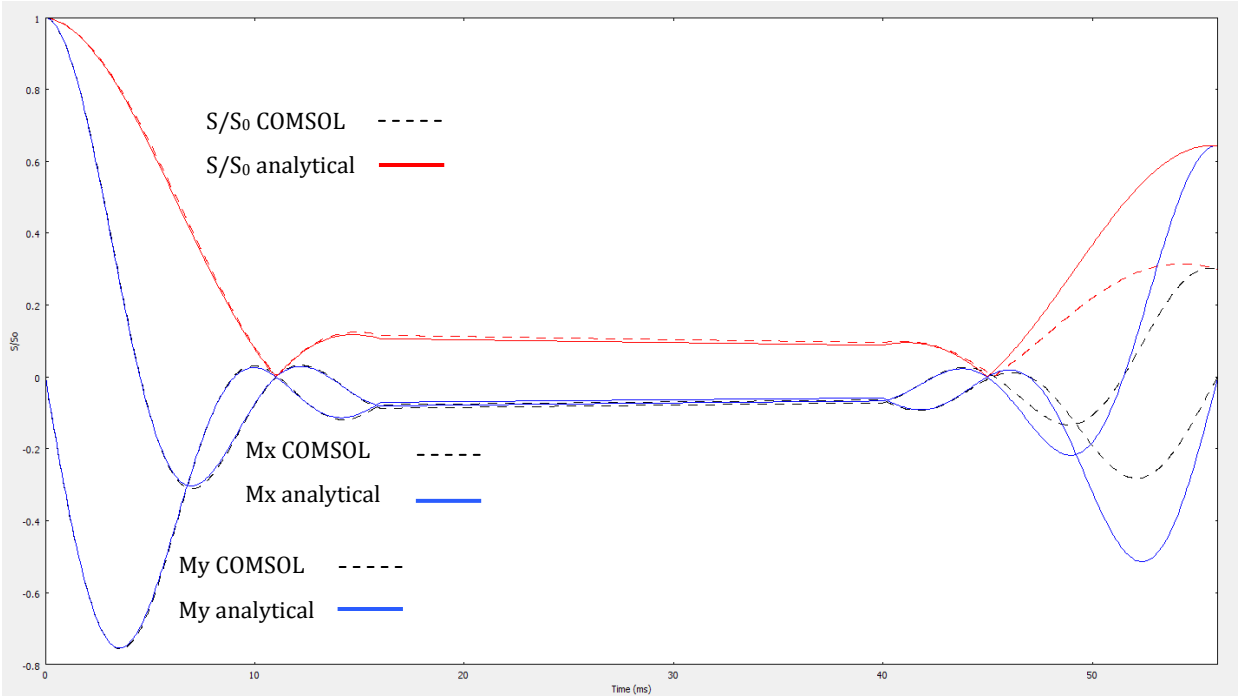

Figure 5.5: Simulation with Diffusion

Here is a contour plot of the domain at time equals 10ms, indicating that diffusion effects are indeed taken into account in the simulation during the first time region.

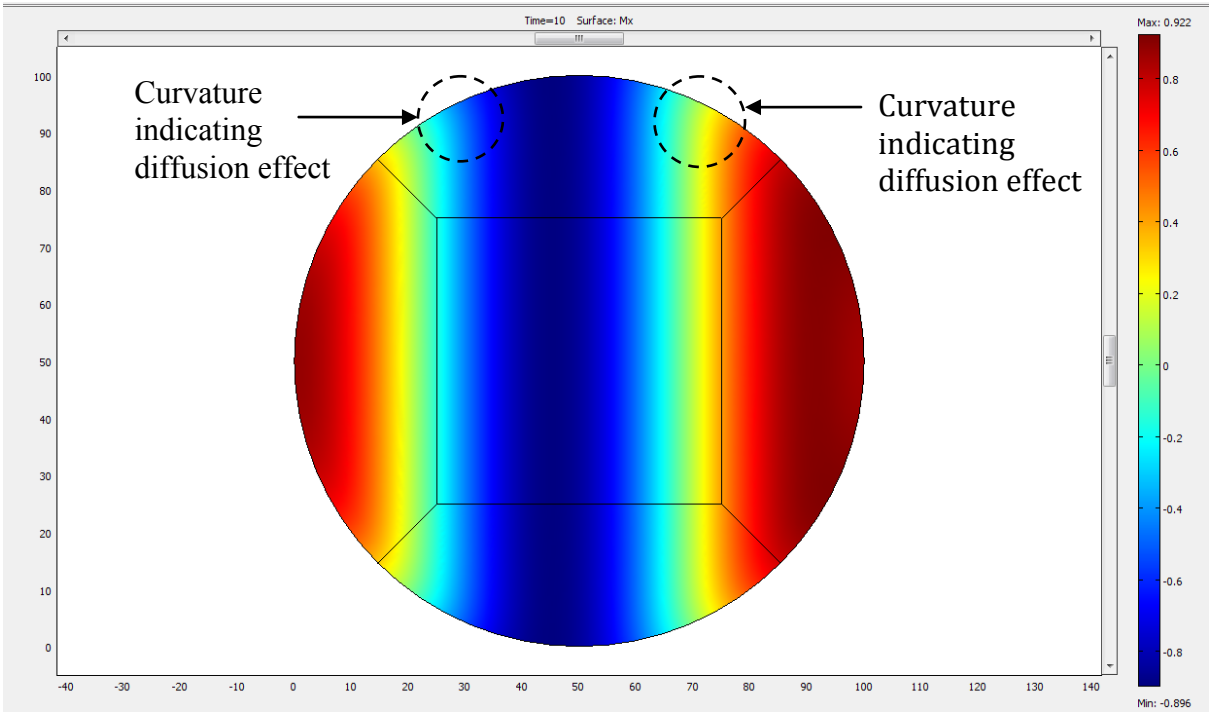

Figure 5.6: Contour Plot with Diffusion

For diffusion validation, the following 2D domain is used:

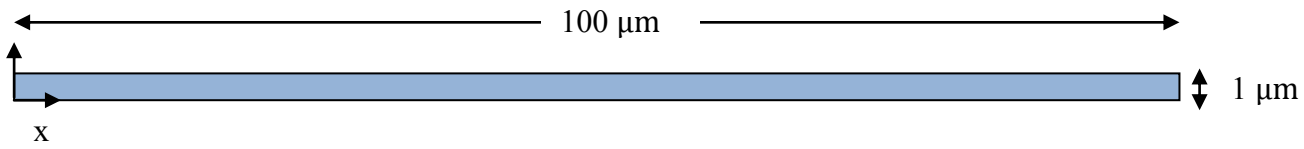

Figure 5.7: Diffusion Validation Domain

We apply a wall boundary condition around all sides, and apply an initial condition of:

$$M_0 = \sin(x\ \pi\ 0.01)\ ,\ \textit{where M is in mT}$$

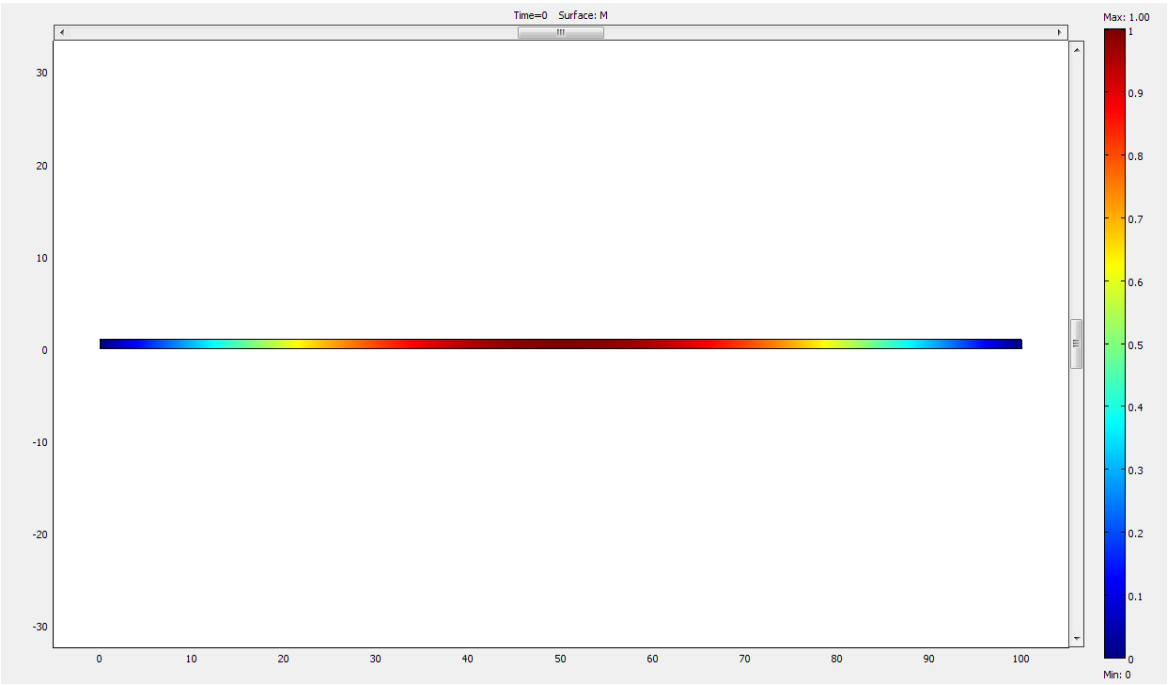

Figure 5.8: Diffusion Validation Contour Plot

The governing equation used for the simulation is:

$$\frac{dM}{dt} = D\frac{d^2M}{dx^2}$$

We pick x=25 m (7=0.5 m for 1D) as the point of interest, and the analytical solution as a function of time using a Fourier series becomes:

$$u(25,t) = \sum_{n=1}^{\infty} 0.02\left(\int_0^{100} \sin(0.01x\pi)\sin(n0.01x\pi)dx\right)\sin(n0.25\pi)\,e^{-\frac{n^2\pi^2\alpha t}{100^2}}$$

Values for magnetization at position x=25μm, choosing diffusion coefficient of 1μm²/ms gives:

Table 5.2: Results for Diffusion Validation

t (ms)	M COMSOL (mT)	M Analytical (mT)
0	0.707107	0.7071
1	0.706409	0.7064
2	0.705713	0.7057
3	0.705017	0.705
4	0.704322	0.7043
5	0.703628	0.7036
6	0.702934	0.7029
7	0.702241	0.7022
8	0.701549	0.7015
9	0.700858	0.7009
10	0.700167	0.7002
11	0.699476	0.6995
12	0.698787	0.6988
13	0.698098	0.6981
14	0.69741	0.6974
15	0.696722	0.6967

The simulation values are in good agreement with the analytical solution as can be observed in the graph:

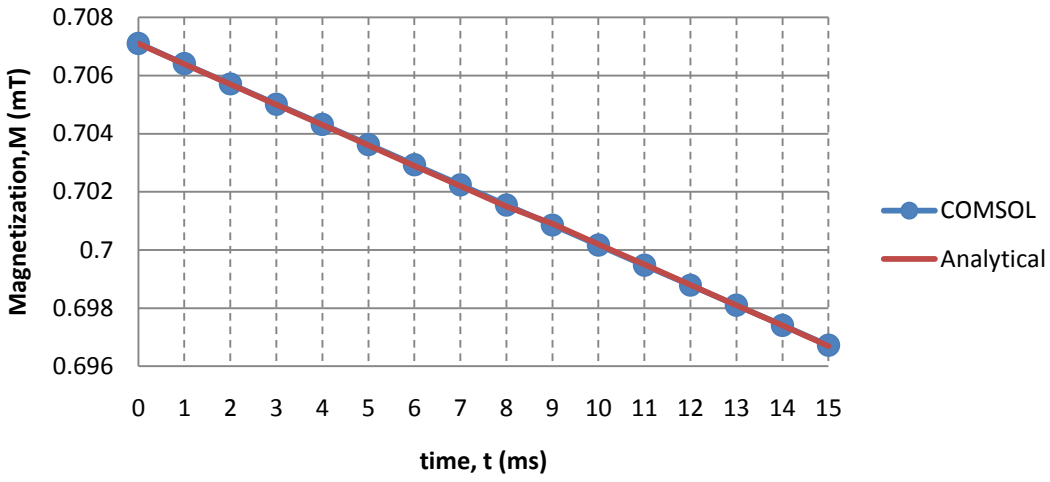

Figure 5.9: Magnetization diffused at x=25μm vs time

6. RESULTS AND DISCUSSION

The direct approach to simulating the signal would be to solve for the governing equations during all three time segments (phi1, phi2, and phi3) for both the water and fat domains simultaneously. However, one can observe that the circular domain is actually independent from the water domain, meaning that it is possible to simulate both separately and then combine them to give the final result. Therefore, an effort was done towards performing a parametric study using only the circle (fat) domain, which was moved along the x direction inside the voxel area, and the magnetization components at time t_E were recorded. This method also saves computational time, and it's also a more efficient way of simulating the signal in the two phase domain, since adding the fat contribution then becomes a matter of post processing. The magnetization components can then be looked up on a graph based on the x coordinate in the domain and b value. The domain has the same mesh and geometric properties as the circular domain in the program validation section, maintaining the same computational parameters, except for further reduction of the time step as shown below.

Table 6.1: Numerical Parameters and Constants for Parametric Circle Simulations

Parameter/Constant	Value
Gyromagnetic ratio for hydrogen (rad/ms*mT)	267.5
t_δ (ms)	16
t_Δ(ms)	40
t_E (ms)	56
T2 for lipid (ms)	127
Mx initial (mT)	1
My initial (mT)	0
Time step (ms)	0.00001 (0.000005 for b=500 and b=600)

The value for the gradient is determined using b as the known variable and the following equation:

$$g = \sqrt{\frac{b}{\gamma^2 \delta^2 (\Delta - \frac{\delta}{3})}}$$

In total, 80 simulations were performed, spanning a total computational time of around 12 days on a 16GB RAM and two 2.66GHz quad core Xeon processor computer. The following results were obtained for a b value range from 0.4 to 0.6 ms/μm2.

Table 6.2: Mx Results for Fat Domain Parametric Simulations

	Mx (mT), b (ms/μm2)			
x (μm)	b=0.3	b=0.4	b=0.5	b=0.6
100	3323.34	2894.92	2524.69	2204.00
250	3323.33	2894.84	2524.58	2203.90
400	3323.31	2894.74	2524.67	2204.05
550	3323.27	2894.64	2524.74	2204.23
700	3323.23	2894.53	2525.09	2205.32
850	3323.18	2894.41	2528.33	2210.71
1000	3323.11	2894.28	2535.42	2216.67
1150	3323.04	2894.14	2541.88	2225.71
1300	3322.96	2894.00	2552.06	2239.72
1450	3322.87	2893.85	2567.34	2260.59
1600	3322.77	2893.70	2590.34	2289.10
1750	3322.66	2893.55	2619.91	2315.40
1900	3322.55	2893.39	2646.41	2353.55
2050	3322.42	2893.24	2686.59	2376.55
2200	3322.29	2895.18	2707.88	2418.75
2350	3322.16	2895.17	2744.99	2448.63
2500	3322.02	2895.14	2774.94	2495.21
2650	3321.87	2895.10	2808.69	2571.11
2800	3321.73	2895.05	2870.65	2585.53
2950	3321.57	2894.99	2936.25	2505.11

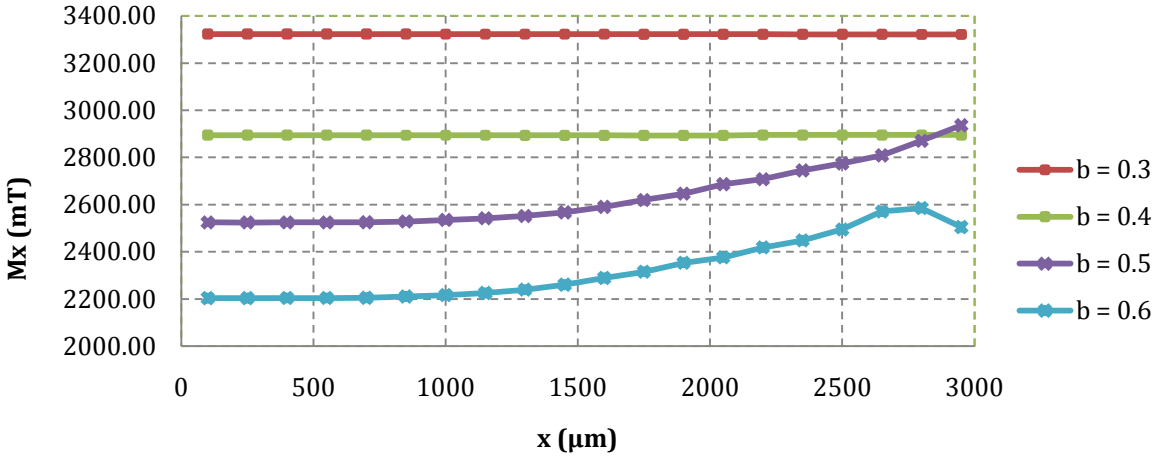

Figure 6.1: Mx at t_E vs x position across domain (b in ms/μm²)

Table 6.3: My Results for Fat Domain Parametric Simulations

	My (mT), b (ms/µm2)			
x (µm)	b=0.3	b=0.4	b=0.5	b=0.6
100	0.00	0.00	0.00	0.00
250	0.00	0.00	-0.01	0.00
400	0.00	0.00	0.20	-1.15
550	0.00	0.00	0.47	0.70
700	0.00	0.00	1.41	1.15
850	0.00	0.00	0.83	5.76
1000	0.00	0.00	7.66	6.21
1150	0.00	0.00	8.20	9.65
1300	0.00	0.00	9.13	6.77
1450	0.00	0.00	11.80	9.76
1600	0.00	0.00	6.11	11.66
1750	0.00	0.00	15.80	106.33
1900	0.00	0.02	115.81	179.30
2050	0.00	0.06	178.42	157.95
2200	0.00	0.00	125.85	72.20
2350	0.00	0.00	84.44	74.24
2500	0.00	0.00	106.85	-19.35
2650	0.00	0.00	-19.92	-111.63
2800	0.00	0.00	-83.49	-174.27
2950	0.00	0.00	-133.24	-502.27

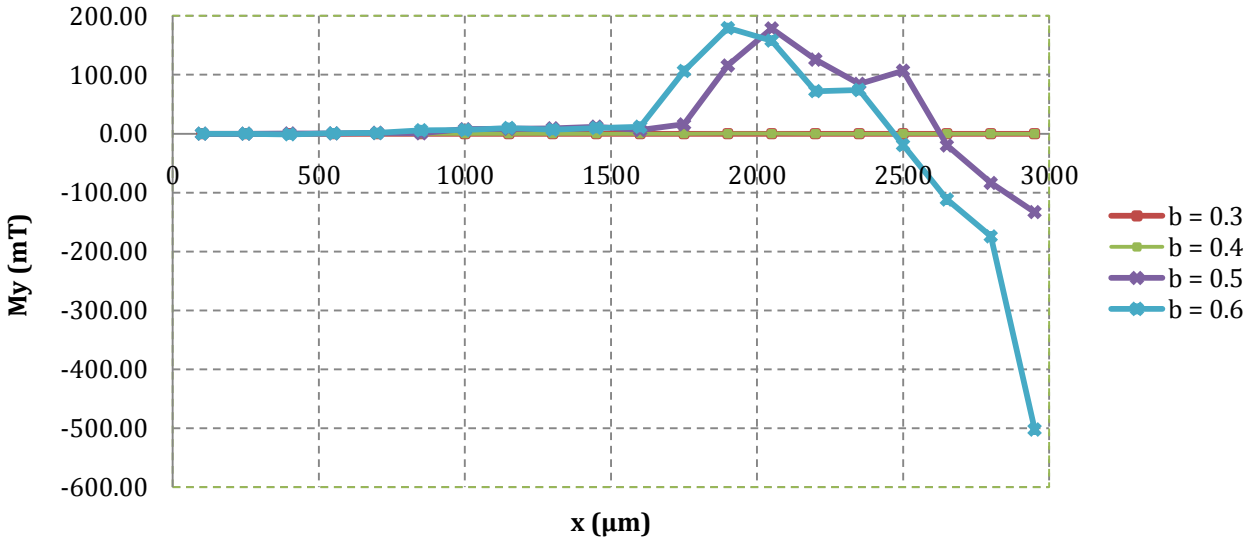

Figure 6.2: My at t_E vs x position across domain (b in ms/µm²)

The results for the parametric study show that for the b values of 0.3 and 0.4, the signal remains almost constant as the circular domain moves to the right. On the other hand, at the higher b values, the signal appears to increase. Knowing that the value of the magnetic field increases while moving towards the right, the phenomena experienced during the higher b values appears to be computational error, mainly divergence of the actual solution as the software solves for the governing equations. The time step might have to be decreased even further to prove this which will undoubtedly increase the computational time significantly, considering that at the 0.000005ms time step, the simulations took close to 3 days to finish for only one b value. In light of the above, and also for simplification purposes, it will be assumed that the signal at any position for each b value will remain constant, taking on the value close to the x=0 position of the domain.

The next step was to simulate the water domain. In total, 9 configurations were used, where the tubes were placed randomly by hand, attempting to achieve random locations. The figure below shows a demonstrative mesh. The other 8 configurations can be found in Appendix B.

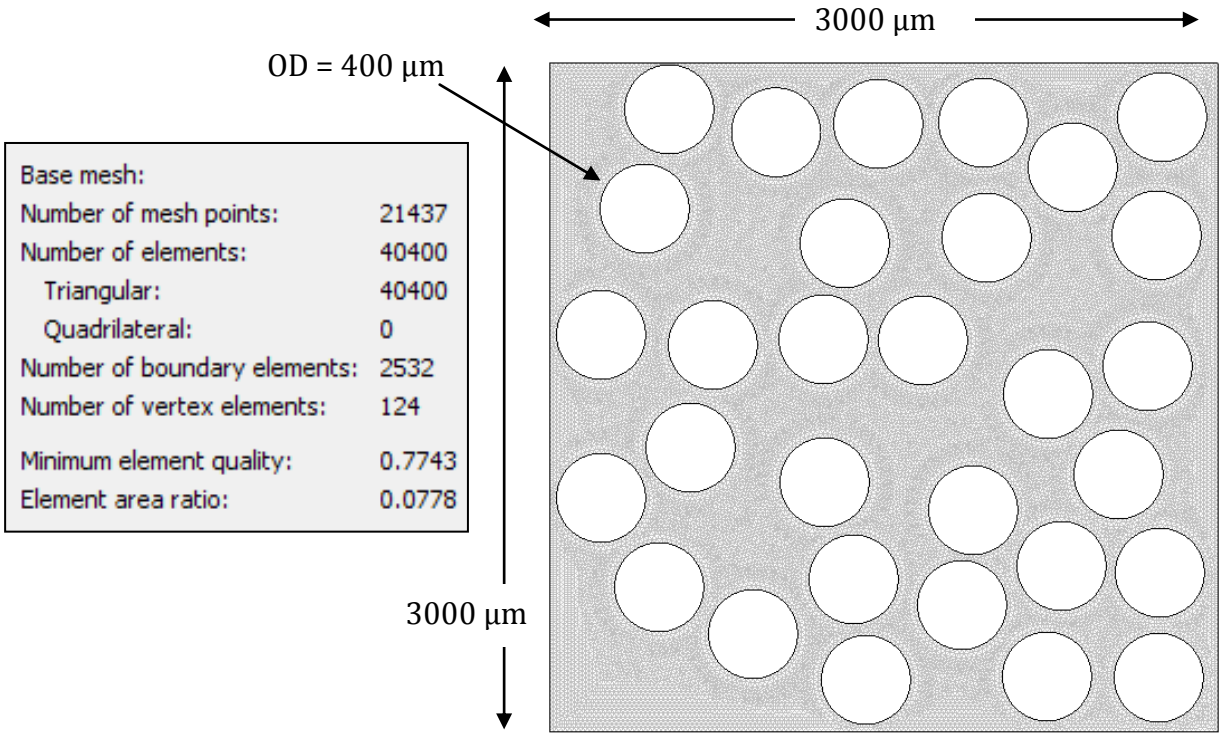

Figure 6.3: Configuration 30a Mesh Statistics

The following is a close up of the domain, displaying element quality:

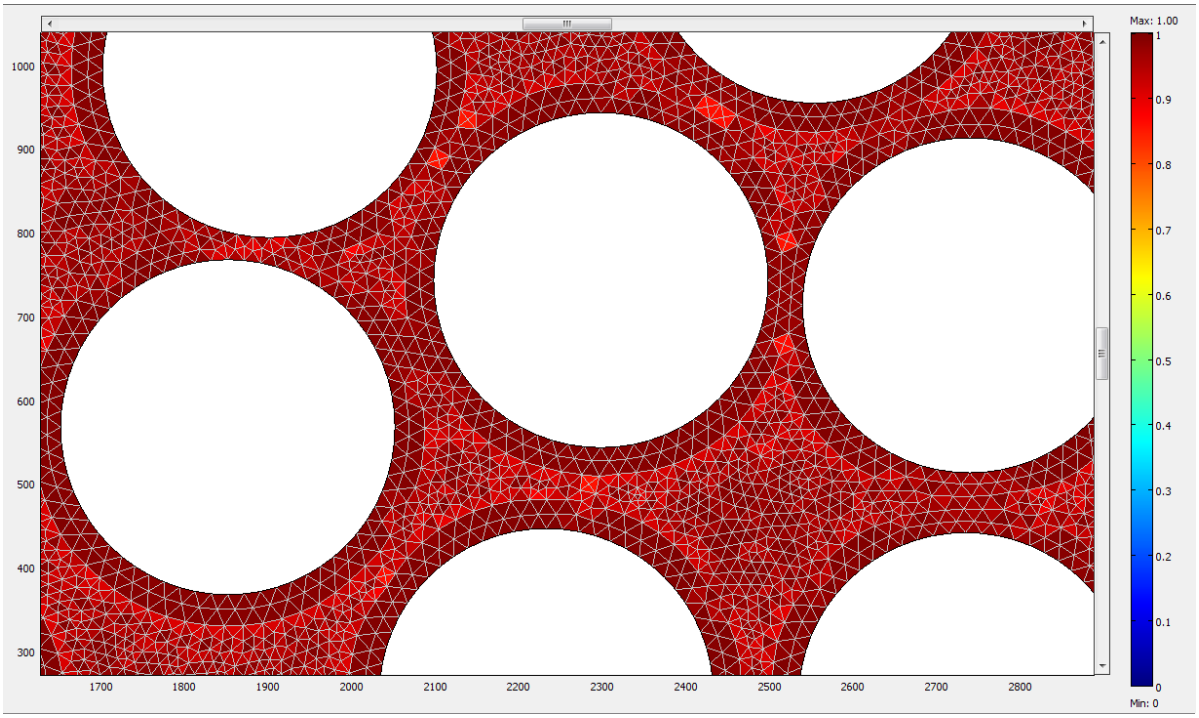

Figure 6.4: Close up of Mesh Element Quality

Table 6.4: Numerical Parameters and Constants for Water Domain Simulations

Parameter/Constant	Value
Gyromagnetic ratio for hydrogen (rad/ms*mT)	267.5
t_δ (ms)	16
t_Δ(ms)	40
t_E (ms)	56
T2 for lipid (ms)	127
T2 for water (ms)	2000
Mx,My initial	1,0
Time step (ms)	0.01
Wall boundary condition, Dirichlett	**M**=0
Boundary condition for outside perimeter	Periodic
Time step (ms)	0.01
Element Type	Triangular
Maximum Element Size Scaling Factor	0.10
Element Growth Rate	1.2
Mesh Curvature Factor	0.2
Mesh Curvature Cutoff	0.0001

In total, there were 36 simulations performed. Appendix C shows example snapshots of a simulation for one of the configurations. The figure below shows the results compared to an experimental value obtained from the research group.

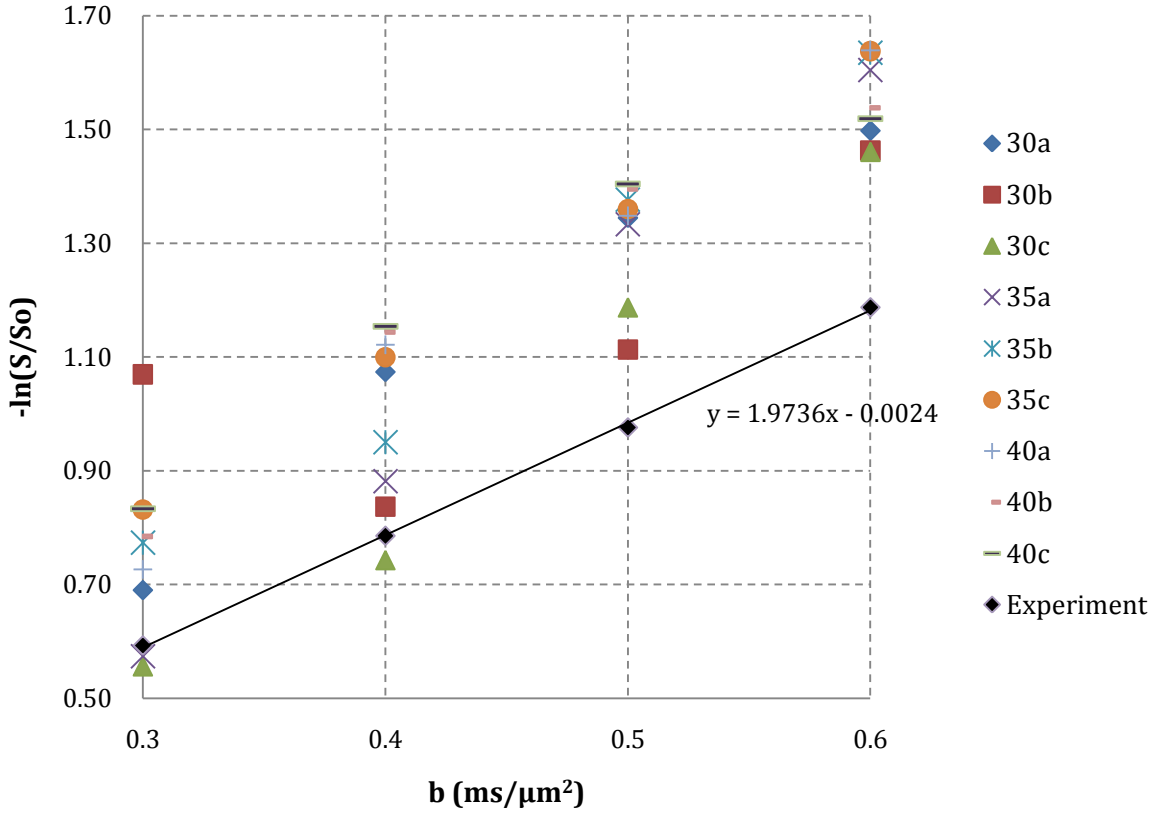

Figure 6.5: Signal Values at t_E for Configurations vs b-factor

As the amount of tubes increases, it appears that the signal values increase as well, compared to the experimental trend line. Also, configurations 30b and 30c seem to be the closest points to the line, indicating that perhaps the experimental configuration had around 30 tubes within the voxel.

Unlike the other points which seem to gradually increase with larger b values, configuration 30b starts at a higher point and then dips. In order to check, the simulation was run again, yielding the same result. This might be an indication that the time step and mesh are not fine enough in order to have stable solutions throughout all potential configurations.

Calculating the slopes of the trend lines results in the apparent diffusion coefficient.

Table 6.5: Apparent Diffusion Coefficients for Configurations and Experiment

Configuration	ADC (μm²/ ms)
30a	2.69
30b	1.46
30c	3.16
35a	3.54
35b	3.01
35c	2.68
40a	2.96
40b	2.51
40c	2.31
Experiment	1.97

The apparent diffusion coefficients are higher than that of the experiment, with the exception of configuration 30b. Increasing the amount of fat inside the domain by adding more tubes more or less decreases the diffusion coefficient values from the simulations. This makes sense, considering that the space gets progressively smaller between the tubes, impeding the diffusion.

Since one of the main goals of the research was to determine the effect of fat on the signal, the percent decrease in signal was calculated using the following equations:

$$S_{without\ fat} = \frac{\sqrt{\left[M_{x\ without\ fat\ tot}(t_E)\right]^2 + \left[M_{y\ without\ fat\ tot}(t_E)\right]^2}}{Area\ of\ Water\ Domain}$$

$$S_{total} = \frac{\sqrt{\left[M_{x\ tot}(t_E)\right]^2 + \left[M_{y\ tot}(t_E)\right]^2}}{Total\ Area}$$

$$\%\ fat\ contribution = \left|\frac{ln(S_{without\ fat}) - ln(S_{total})}{ln(S_{without\ fat})}\right| x100$$

The following figure illustrates the effect of the fat for each configuration and b value simulated:

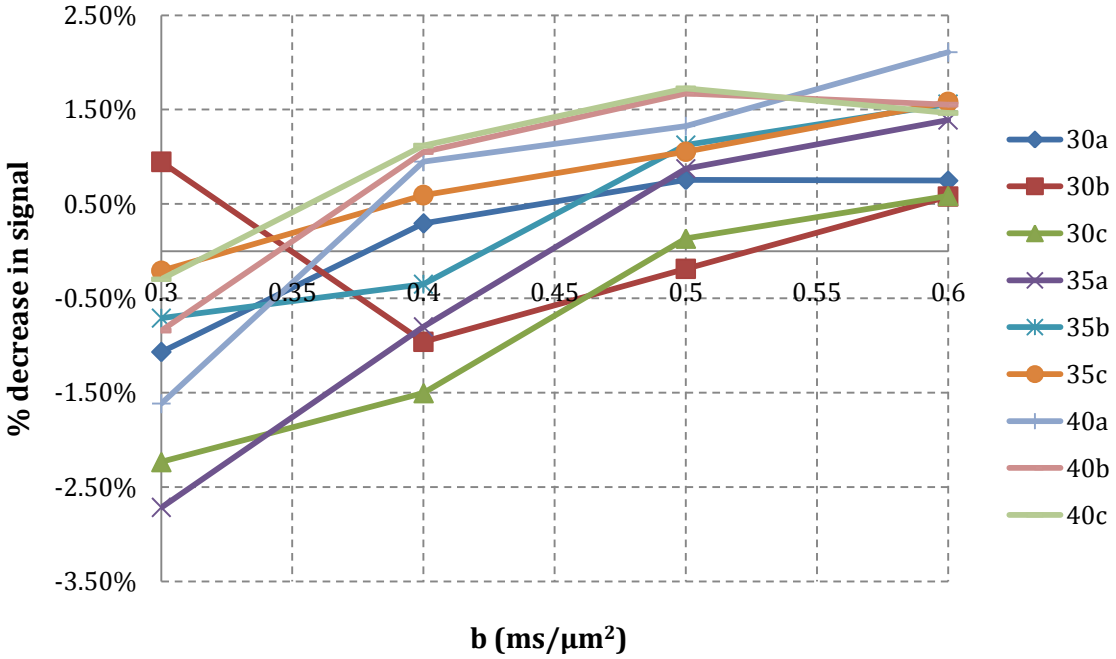

Figure 6.6: Percent Decrease in Signal by Including Fat

As can be seen by the graph, the percentage effect is low throughout the b range values, enough to say that the contribution of fat for the 9 configurations appears to be negligible. There is a general trend of a decrease in the signal caused by fat as the b values increase.

Furthermore, increasing the amount of tubes appears to decrease the signal as well. With more tubes, there is undoubtedly an increase of fat relative to the water domain, which allows for a greater influence to the signal decay.

There is a spike in the 30b configuration which was carried over from the signal results (refer to Figure 6.5).

7. CONCLUSIONS

Based on percent contribution, the amount of fat in the configuration domains seems to have an almost negligible effect on the signal, especially as b values are increased. The reason why the fat has a negligible effect on the signal might be that the domain area of fat is significantly smaller than that of water. For the 40 tube case, the fat consists of only 8% of the total domain area. Figure 6.6 seems to be in agreement with the hypothesis, since it appears that there is a decrease in the signal compared to an all-water domain as more tubes are added. Due to fat's significantly shorter T2 value compared to pure water (127ms vs 2000ms), it is to be expected that the signal will decay faster and more prominently as it takes on a larger portion of the domain of interest.

By adding more tubes, the spacing becomes tighter, and the fat, which has a lower diffusion coefficient than water, will have an effect on the apparent diffusion coefficient (lowering it towards the experimental value). When modeling a domain of skeletal muscle (figure 2.1), the muscle fibers would be tightly packed, making it harder for water to diffuse in between the fibers (endomysium region) and this will undoubtedly reduce the diffusion coefficient.

There seems to be some computational error occurring in both the parametric fat domain and pure water domain simulations. Considering that the time step and mesh for the parametric circle domain case are very small compared to the water domain cases, and observing computational error in the prior, it seems likely that these factors will affect the accuracy of the simulations. The extent to which it will do so is unknown at this point. The general limitation involved is computational effort, since the domain is quite large with a small time step. Regardless, there is a consistent trend shown in Figure 6.5 throughout all 9 configurations, save for the b=300ms/μm2 value for 30b as mentioned before.

8. FUTURE WORK

There are improvements and further things to explore based on the results of the research presented in this paper, as listed below:

- Verify that the signal for the parametric circle domain study does remain constant for any position within the gradient at any b value. Therefore, perform the same simulation with smaller time step and wider range of b values. This could then be used to show a relationship between the signal value at time echo with the b value.

- Perform a more extensive simulation with many tube configurations, changing the number and arrangement of the tubes inside the domain. As mentioned in the previous section, the time step and mesh size should also be decreased in order to improve accuracy of the simulations. Since this is a computationally intensive step, it would be best to use a super computer.

- Create an experiment that has even smaller tubes and less wall thickness in order to validate a model configuration which will be closer to actual muscle fiber tissue. As mentioned before, the limitation involved here is in finding tubes that are manufactured that small. Something else to consider in the future is to include water permeability in the model as well, which would simulate water diffusing between the muscle fibers and the endomysium.

REFERENCES

[1] Jason, A. C. *Effects of Fat Content on Diffusion of Water in Fish Muscle*. Journal of the Science of Food and Agriculture, Vol. 16, 1965.

[2] Karampinos, King, Sutton, and Georgiadis. *In Vivo Study of Cross-Sectional Skeletal Muscle Fiber Asymmetry with Diffusion-Weighted MRI*. Engineering in Medicine and Biology Society, Lyon, France, August, 2007.

[3] Le Bihan, et al. *Diffusion Tensor Imaging: Concepts and Applications*. Journal of Magnetic Resonance Imaging, 2001.

[4] Liang, Zhi-Pei, and Lauterbur, Paul C. *Principles of Magnetic Resonance Imaging: A Signal Processing Perspective*. IEEE Press. New York, 2000.

[5] Mattiello, Basser, and Le Bihan. *Analytical Expressions for the b Matrix in NMR Diffusion Imaging and Spectroscopy*. Journal of Magnetic Resonance, Series A, 1994.

[6] Stejskal and Tanner. *Spin Diffusion Measurements: Spin Echoes in the Presence of a Time-Dependent Field Gradient*. The Journal of Chemical Physics, Vol. 42, January 1965.

[7] Torrey, H. C. *Bloch Equations with Diffusion Terms*. Physics Department, Rutgers University, New Brunswick, New Jersey, 1956

Figure 2.1:

Top: Fox, S.I. *Human Physiology*, 4th Ed.Wm.C. Brown, publ.
Bottom: "Reasons to Strength Train #47." http://eugenization.com/reasons-to-strength-train-47

APPENDIX A: DERIVATION OF EQUATIONS IN PROGRAM VALIDATION

General governing equation:

$$\frac{dM_x}{dt} = -\left(\frac{1}{T_2}\right) M_x + (\gamma g x) M_y$$

$$\frac{dM_y}{dt} = -(\gamma g x) M_x - \left(\frac{1}{T_2}\right) M_y$$

Grouping coefficients,

$$\alpha = \frac{1}{T_2}, \qquad \beta = \gamma g x$$

Substituting,

$$\frac{dM_x}{dt} = -\alpha M_x + \beta M_y$$

$$\frac{dM_y}{dt} = -\beta M_x - \alpha M_y$$

Assume a solution of the form,

$$M_x = Ae^{\lambda t}, \qquad M_y = Be^{\lambda t}$$

Substituting back into the ODE,

$$A\lambda e^{\lambda t} = -\alpha A e^{\lambda t} + \beta B e^{\lambda t}$$

$$B\lambda e^{\lambda t} = -\beta A e^{\lambda t} - \alpha B e^{\lambda t}$$

Leads to the algebraic system,

$$(-\alpha - \lambda)A + \beta B = 0$$

$$-\beta A + (-\alpha - \lambda)B = 0$$

$$\begin{vmatrix} -\alpha - \lambda & \beta \\ -\beta & -\alpha - \lambda \end{vmatrix} = 0$$

$$(-\alpha - \lambda)^2 + \beta^2 = 0$$

$$a^2 + 2\alpha\lambda + \lambda^2 + \beta^2 = 0$$

$$\lambda^2 + 2\alpha\lambda + (a^2 + \beta^2) = 0$$

$$\frac{-2\alpha \pm \sqrt{(2\alpha)^2 - 4(a^2 + \beta^2)}}{2}$$

$$\lambda = -\alpha \pm i\beta$$

Using the positive sign,

$$-i\beta A + \beta B = 0$$

$$-\beta A - i\beta B = 0$$

$$A = \beta, \qquad B = i\beta$$

Plugging back in to solution form,

$$M_x = \beta e^{(-\alpha+i\beta)t}, \qquad M_y = i\beta e^{(-\alpha+i\beta)t}$$

Using Euler's formula,

$$M_x = \beta e^{-\alpha t}[\cos\beta t + i\sin\beta t]$$

$$M_y = \beta e^{-\alpha t}[-\sin\beta t + i\cos\beta t]$$

The two real solutions are:

$$M_x = \beta e^{-\alpha t}\cos\beta t$$

$$M_y = -\beta e^{-\alpha t}\sin\beta t$$

The two imaginary solutions are:

$$M_x = \beta e^{-\alpha t}\sin\beta t$$

$$M_y = \beta e^{-\alpha t}\cos\beta t$$

General solution:

$$M_x = \beta e^{-\alpha t}[c_1\cos\beta t + c_2\sin\beta t]$$

$$M_y = \beta e^{-\alpha t}[-c_1\sin\beta t + c_2\cos\beta t]$$

- For time equals zero to t_δ, we apply initial condition of Mx=1, My=0:

$$1 = \beta c_1, \qquad c_1 = \frac{1}{\beta}$$
$$0 = \beta c_2, \qquad c_2 = 0$$

$$M_x = e^{-\alpha t}\cos\beta t$$
$$M_y = -e^{-\alpha t}\sin\beta t$$

Substituting back,

$$M_x = e^{-(\frac{t}{T_2})} \cos(\gamma g x t)$$
$$M_y = -e^{-(\frac{t}{T_2})} \sin(\gamma g x t)$$

Expression for the total magnetization component in x and y directions are then given as follows, where h(x) is the vertical length function of the domain with respect to the position x, with lower and upper bounds x_0 and x respectively.

$$M_{x\,tot}(t) = e^{-(\frac{t}{T_2})} \int_{x_0}^{x} h(x) \cos(\gamma g x t)\, dx$$
$$M_{y\,tot}(t) = -e^{-(\frac{t}{T_2})} \int_{x_0}^{x} h(x) \sin(\gamma g x t)\ dx$$

The signal is defined as:

$$S(t) = \sqrt{[M_{x\,tot}(t)]^2 + \left[M_{y\,tot}(t)\right]^2}$$

$$S(t) = \sqrt{\left[e^{-(\frac{t}{T_2})} \int_{x_0}^{x} h(x) \cos(\gamma g x t)\, dx\right]^2 + \left[-e^{-(\frac{t}{T_2})} \int_{x_0}^{x} h(x) \sin(\gamma g x t)\ dx\right]^2}$$

$$S(t) = e^{-(\frac{t}{T_2})} \sqrt{\left[\int_{x_0}^{x} h(x) \cos(\gamma g x t)\, dx\right]^2 + \left[\int_{x_0}^{x} h(x) \sin(\gamma g x t)\ dx\right]^2}$$

Since we will be using Mx=1 and My=0 for the initial condition, the signal at time zero will result in the area integration:

$$S_0 = S(t = 0) = \int_{x_0}^{x} h(x)dx = Area$$

- For time=t_δ, the signal will only experience decay, resulting in the following solution:

$$\mathrm{M_{x\,tot}(t) = e^{-(\frac{t}{T_2})} \int_{x_0}^{x} h(x) \cos(\gamma g x t_\delta)\, dx}$$
$$\mathrm{M_{y\,tot}(t) = -e^{-(\frac{t}{T_2})} \int_{x_0}^{x} h(x) \sin(\gamma g x t_\delta)\, dx}$$

- For the time region starting at time=t_Δ, it is simpler to derive an equation starting at t=0, and setting the initial Mx and My components equal to the last time step,

$$M_x = \beta e^{-\alpha t}[c_1 \cos \beta t + c_2 \sin \beta t]$$

$$M_y = \beta e^{-\alpha t}[-c_1 \sin \beta t + c_2 \cos \beta t]$$

$$M_x(t_\Delta) = \beta c_1, \qquad c_1 = \frac{M_x(t_\Delta)}{\beta}$$

$$M_y(t_\Delta) = \beta c_2, \qquad c_2 = \frac{M_y(t_\Delta)}{\beta}$$

Substituting back in,

$$M_x = e^{-(\frac{t}{T_2})}[M_x(t_\Delta)\cos(-\gamma g x t) + M_y(t_\Delta)\sin(-\gamma g x t)]$$

$$M_y = e^{-(\frac{t}{T_2})}[-M_x(t_\Delta)\sin(-\gamma g x t) + M_y(t_\Delta)\cos(-\gamma g x t)]$$

APPENDIX B: MESH CONFIGURATIONS AND STATISTICS

Base mesh:	
Number of mesh points:	21254
Number of elements:	40046
Triangular:	40046
Quadrilateral:	0
Number of boundary elements:	2520
Number of vertex elements:	124
Minimum element quality:	0.8455
Element area ratio:	0.1087

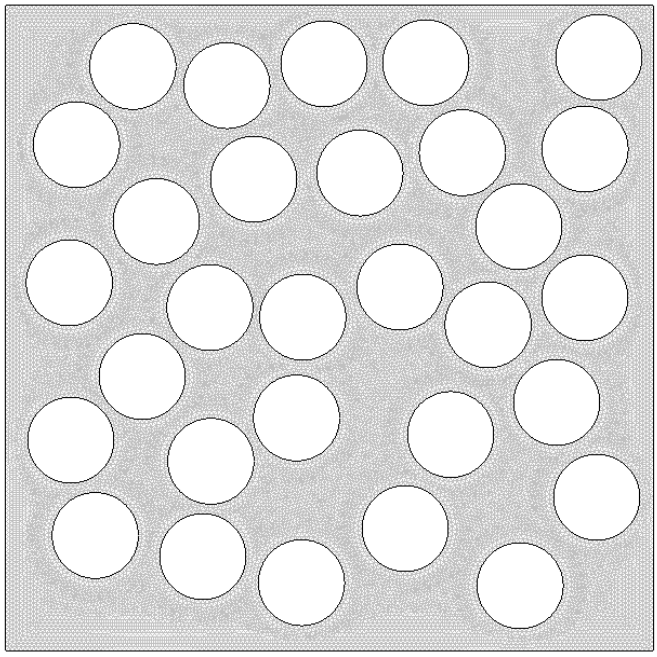

Figure B.1: Configuration 30b Mesh Statistics

Base mesh:	
Number of mesh points:	21068
Number of elements:	39674
Triangular:	39674
Quadrilateral:	0
Number of boundary elements:	2520
Number of vertex elements:	124
Minimum element quality:	0.8479
Element area ratio:	0.1253

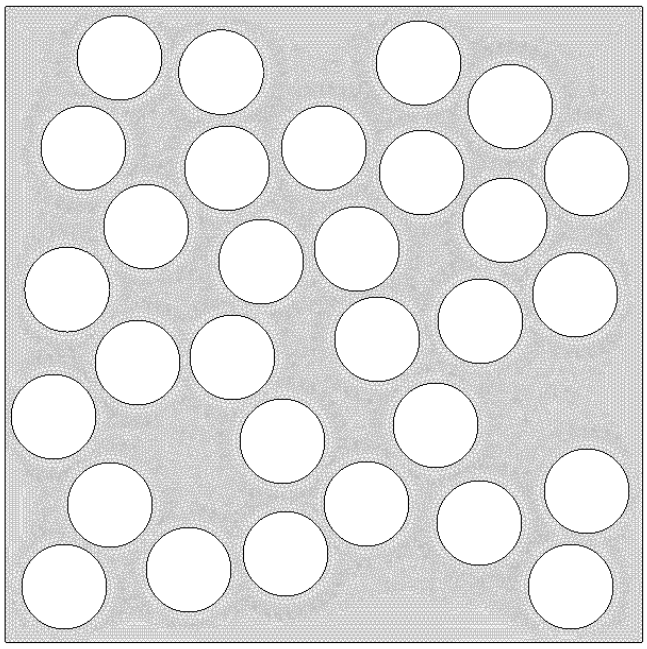

Figure B.2: Configuration 30c Mesh Statistics

Base mesh:	
Number of mesh points:	18852
Number of elements:	34932
Triangular:	34932
Quadrilateral:	0
Number of boundary elements:	2840
Number of vertex elements:	144
Minimum element quality:	0.7951
Element area ratio:	0.1090

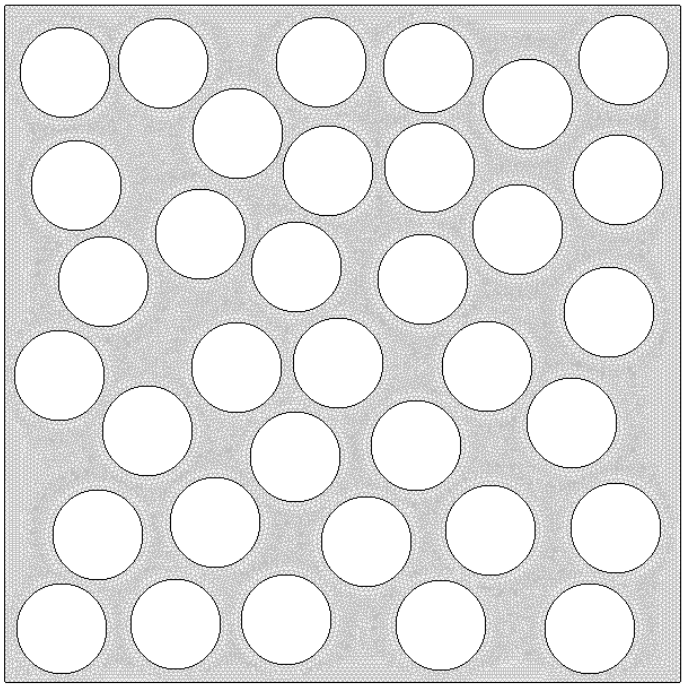

Figure B.3: Configuration 35a Mesh Statistics

Base mesh:	
Number of mesh points:	18977
Number of elements:	35182
Triangular:	35182
Quadrilateral:	0
Number of boundary elements:	2840
Number of vertex elements:	144
Minimum element quality:	0.8442
Element area ratio:	0.0946

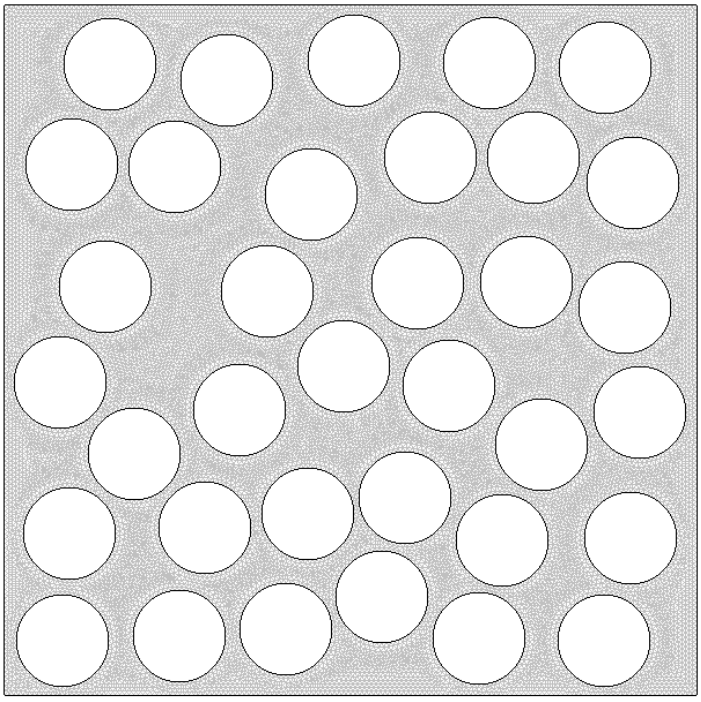

Figure B.4: Configuration 35b Mesh Statistics

Base mesh:	
Number of mesh points:	18756
Number of elements:	34740
Triangular:	34740
Quadrilateral:	0
Number of boundary elements:	2840
Number of vertex elements:	144
Minimum element quality:	0.8430
Element area ratio:	0.0774

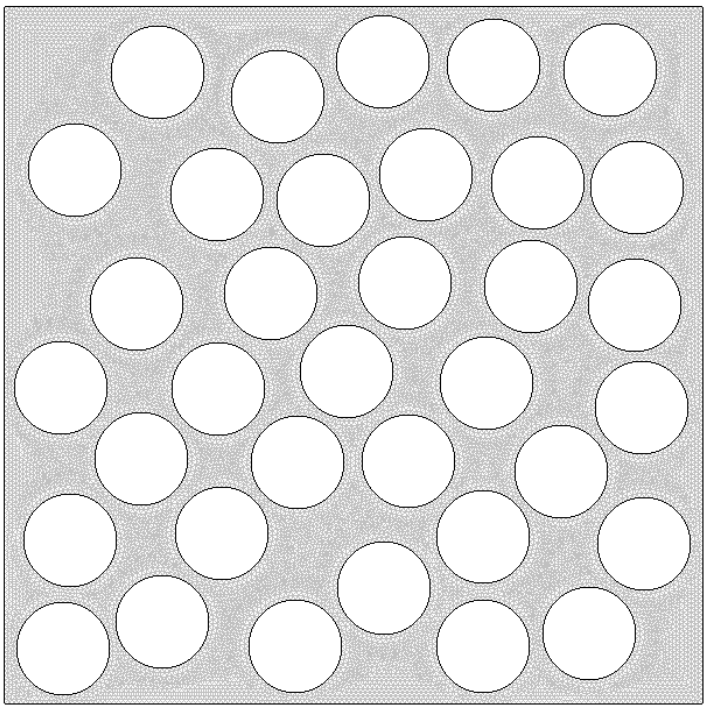

Figure B.5: Configuration 35c Mesh Statistics

Base mesh:	
Number of mesh points:	16148
Number of elements:	29214
Triangular:	29214
Quadrilateral:	0
Number of boundary elements:	3160
Number of vertex elements:	164
Minimum element quality:	0.8451
Element area ratio:	0.0966

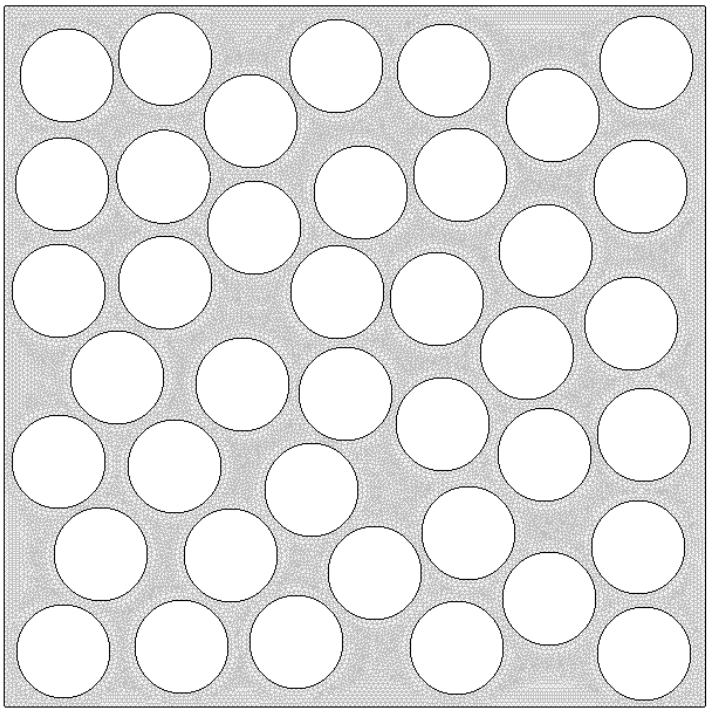

Figure B.6: Configuration 40a Mesh Statistics

Base mesh:	
Number of mesh points:	16180
Number of elements:	29278
Triangular:	29278
Quadrilateral:	0
Number of boundary elements:	3160
Number of vertex elements:	164
Minimum element quality:	0.8318
Element area ratio:	0.0884

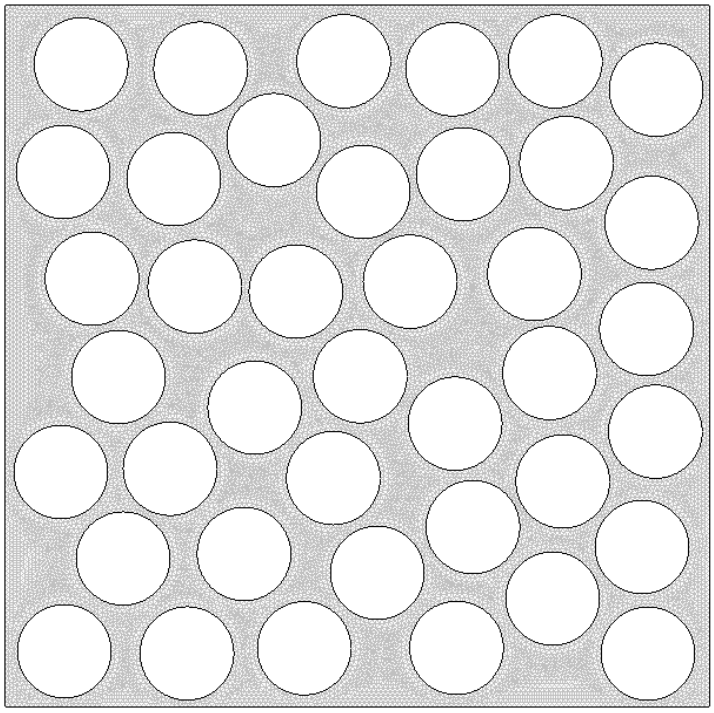

Figure B.7: Configuration 40b Mesh Statistics

Base mesh:	
Number of mesh points:	16279
Number of elements:	29476
Triangular:	29476
Quadrilateral:	0
Number of boundary elements:	3160
Number of vertex elements:	164
Minimum element quality:	0.8304
Element area ratio:	0.1211

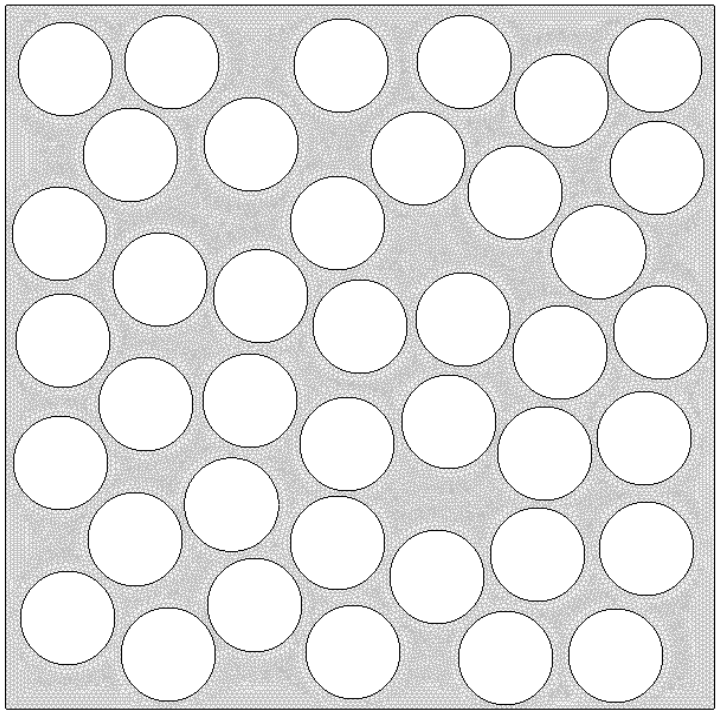

Figure B.8: Configuration 40c Mesh Statistics

APPENDIX C: RESULTS SAMPLE

The following are 3D contours of Mx (mT) for configuration 30a at b = 0.3ms/μm².

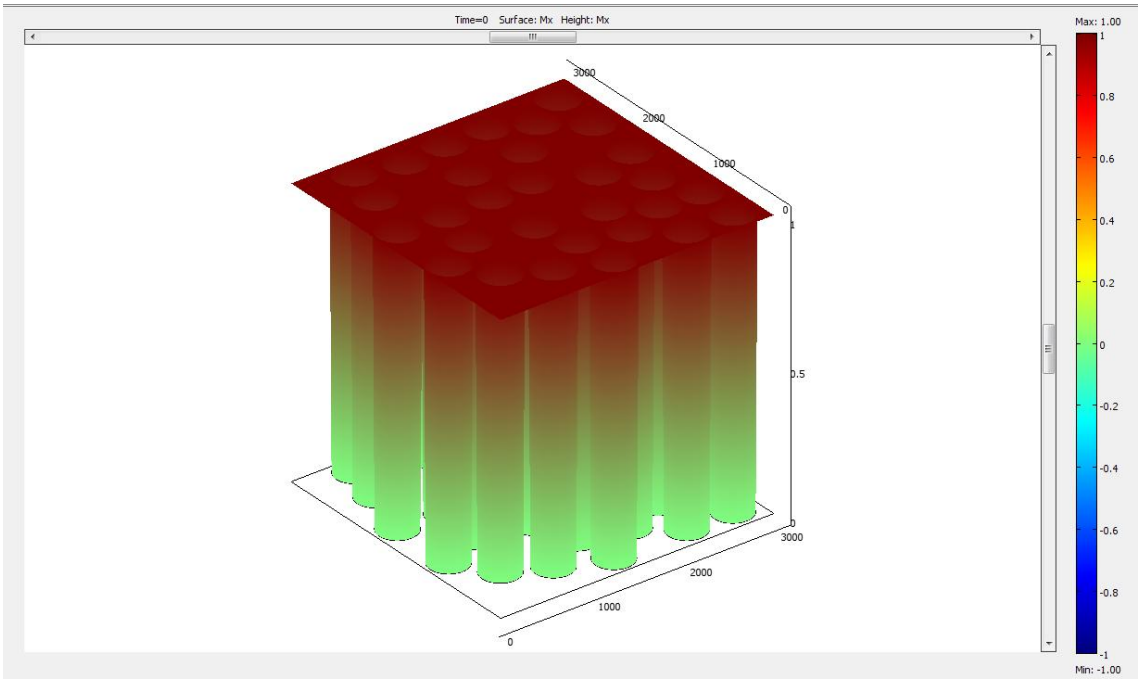

Figure C.1: Mx 3D Contour at t=0ms

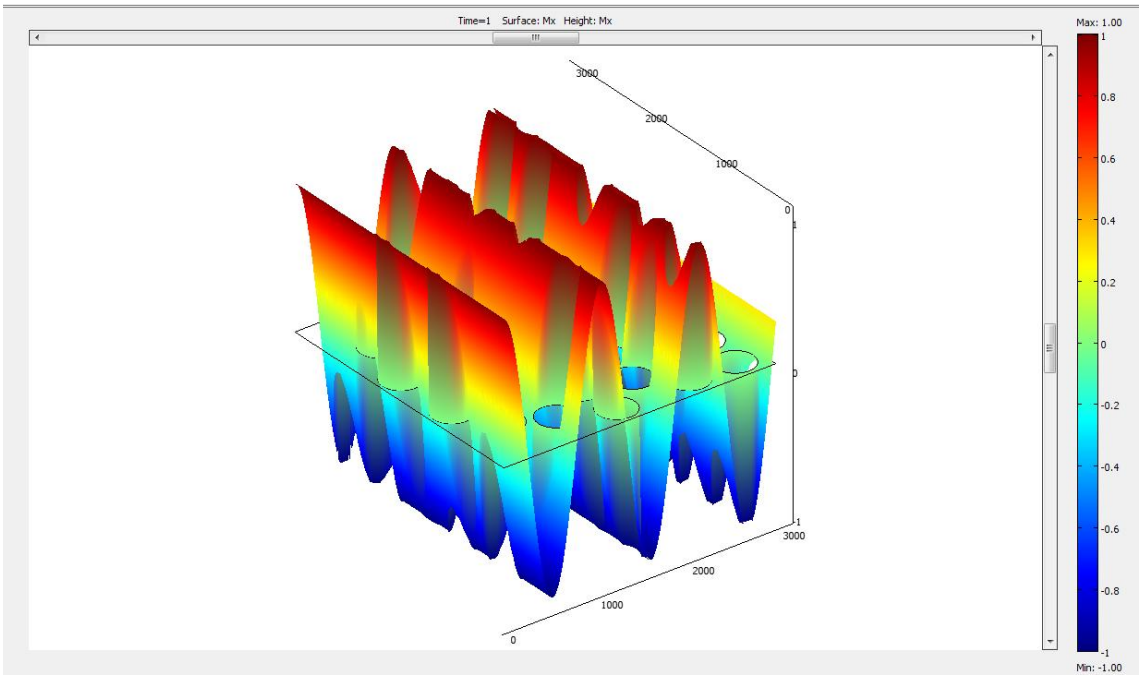

Figure C.2: Mx 3D Contour at t=1ms

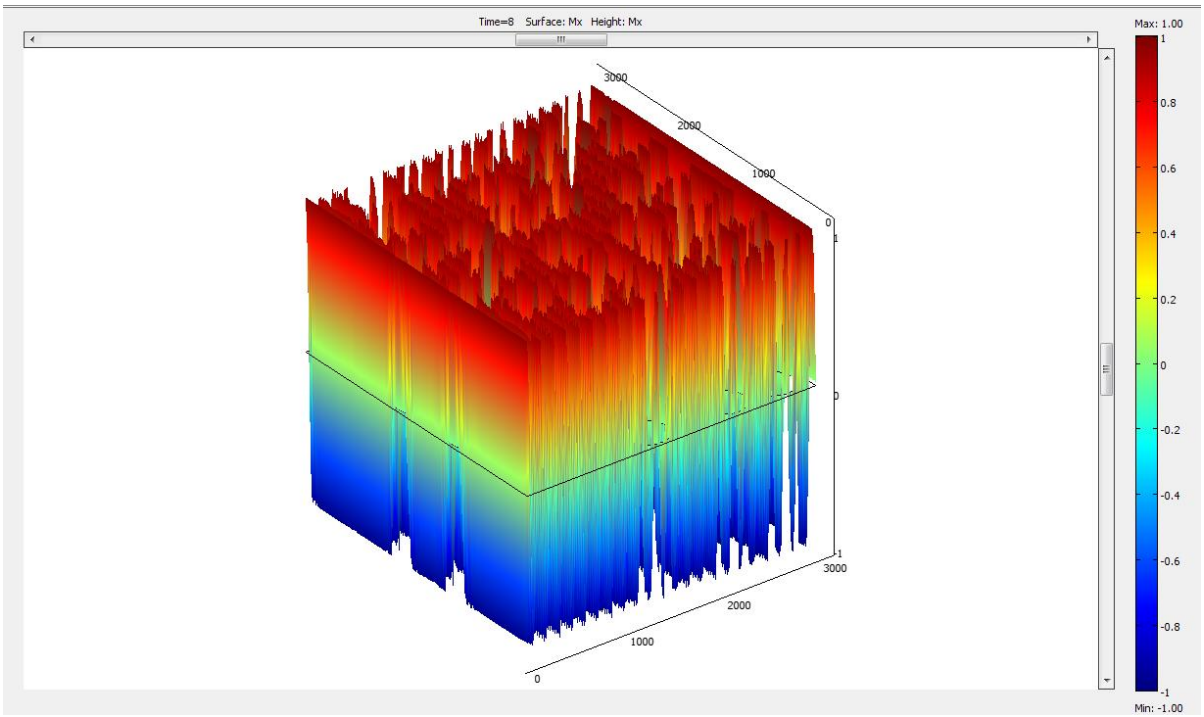

Figure C.3: Mx 3D Contour at t=8ms

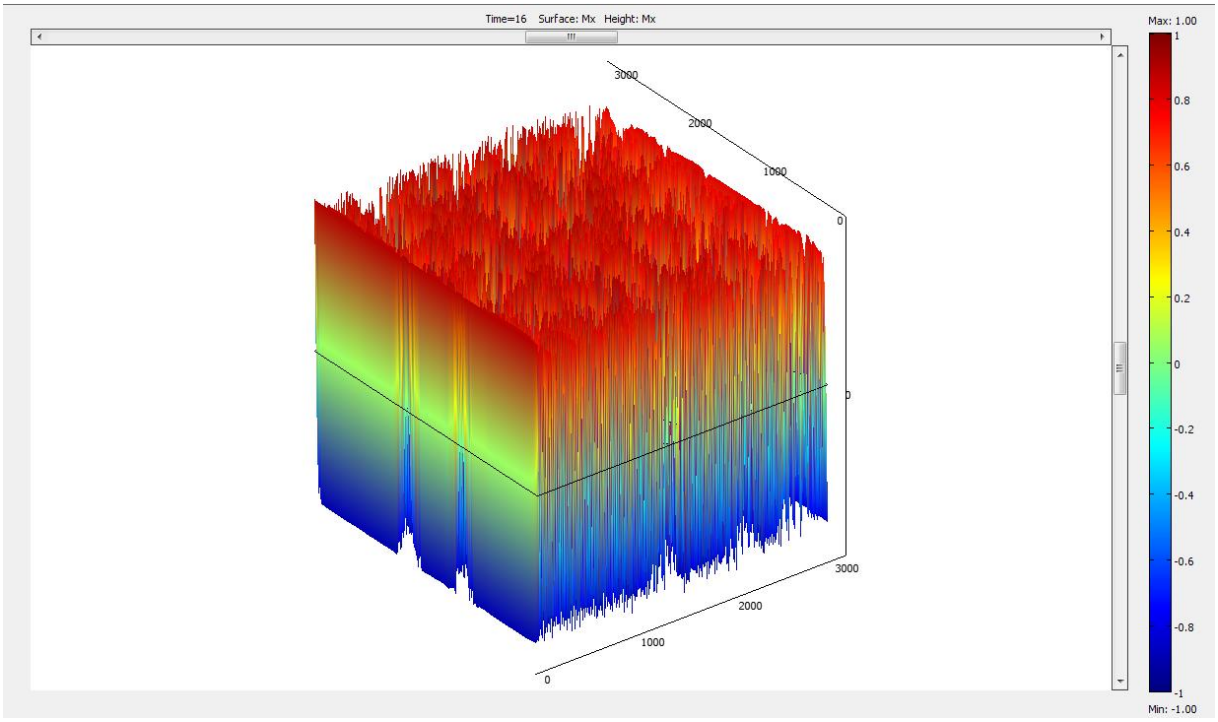

Figure C.4: Mx 3D Contour at t=16ms (start of free relaxation)

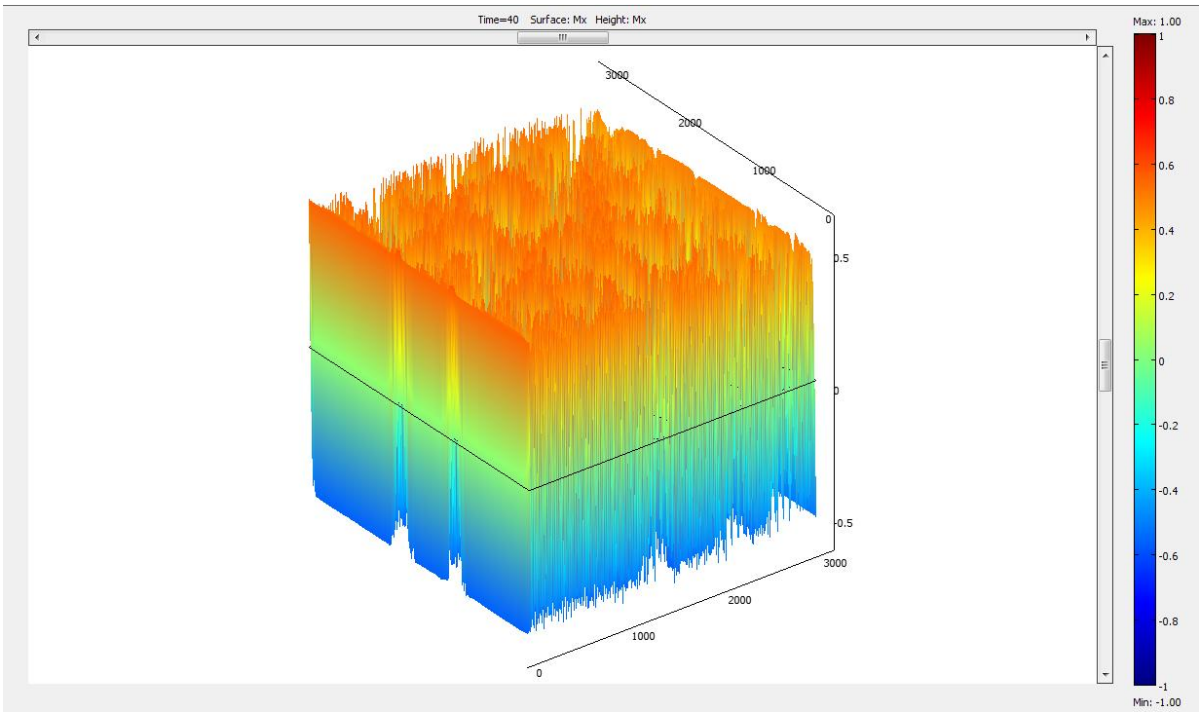

Figure C.5: Mx 3D Contour at t=40ms (negative gradient applied)

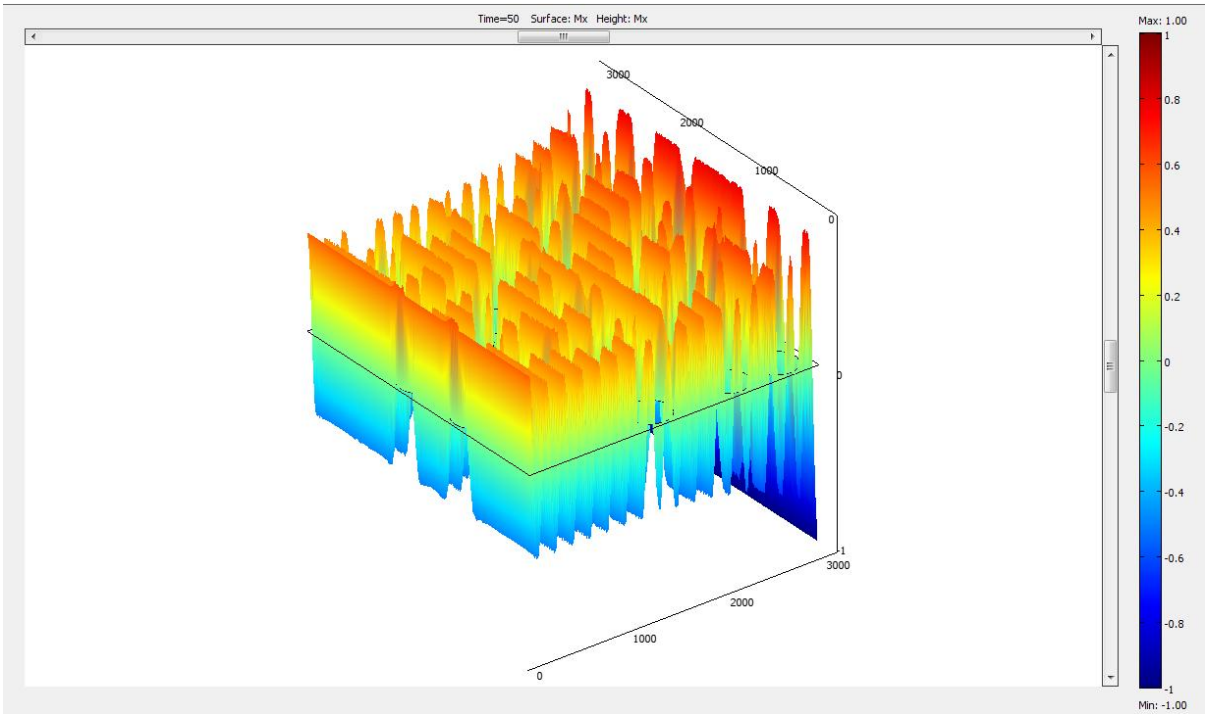

Figure C.6: Mx 3D Contour at t=50ms

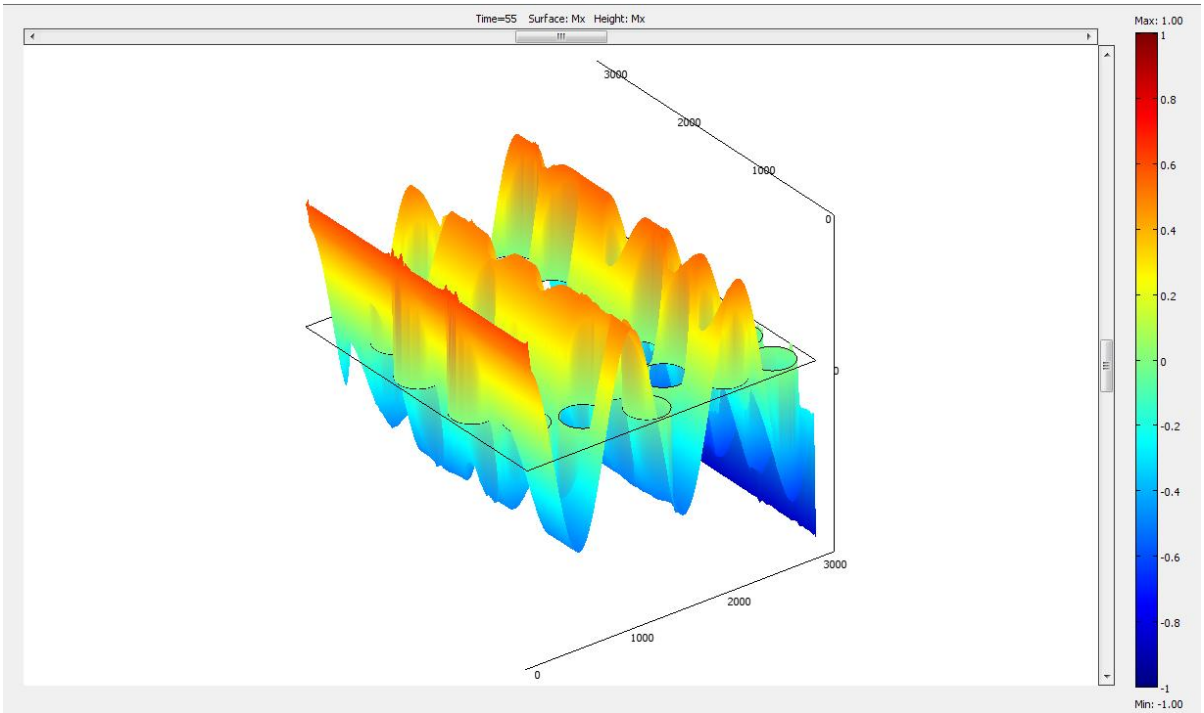

Figure C.7: Mx 3D Contour at t=55ms

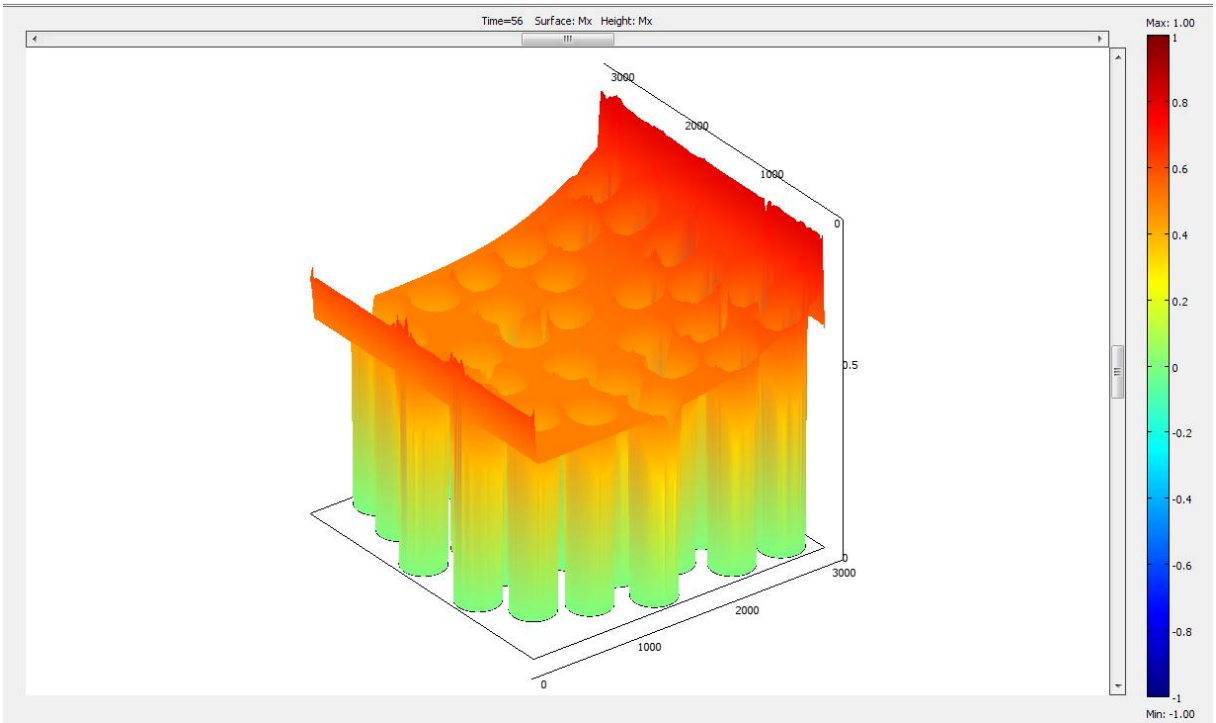

Figure C.8: Mx 3D Contour at t=56ms (signal acquisition at echo)